# Quality Controlling Surf Zone Acoustic Doppler Velocimeter Observations to Estimate the Turbulent Dissipation Rate

FALK FEDDERSEN

*Scripps Institution of Oceanography, La Jolla, California*

(Manuscript received 16 March 2010, in final form 29 July 2010)

ABSTRACT

High-quality measurements of the turbulent dissipation rate $\bar{\epsilon}$ are required to diagnose field surf-zone turbulence budgets. Quality control (QC) methods are presented for estimating surf zone $\bar{\epsilon}$ with acoustic Doppler velocimeter (ADV) data. Bad ADV velocity data points are diagnosed with both the ADV signal strength (SS) and correlation (CORR). The fraction of bad SS data points ($\delta_{\mathrm{SS}}$) depends inversely upon the wave-amplitude-normalized transducer distance below the mean sea surface. The fraction of bad CORR data points $\delta_{\mathrm{CORR}}$ can be elevated when $\delta_{\mathrm{SS}}$ is low. The $\delta_{\mathrm{CORR}}$ depends inversely upon the wave-amplitude-normalized sensing volume distance below the mean sea surface, and also increases with increased wave breaking, consistent with turbulence- and bubble-induced Doppler noise. Velocity spectra derived from both ''patched'' and ''interpolated'' time series are used to estimate $\bar{\epsilon}$. Two QC tests, based upon the properties of a turbulent inertial subrange, are used to reject bad $\bar{\epsilon}$ data runs. The first test checks that the vertical velocity spectrum's power-law exponent is near $-5/3$. The second test checks that a ratio $R$ of horizontal and vertical velocity spectra is near 1. Over all $\delta_{\mathrm{CORR}}$, 70% of the patched and interpolated data runs pass these tests. However, for larger $\delta_{\mathrm{CORR}} > 0.1$ (locations higher in the water column), 50% more patched than interpolated data runs pass the QC tests. Previous QC methods designed for wave studies are not appropriate for $\bar{\epsilon}$ QC. The results suggest that $\bar{\epsilon}$ can be consistently estimated over the lower 60% of the water column and >0.1 m above the bed within a saturated surf zone.

## 1. Introduction

Surf zone turbulence vertically mixes momentum, tracers, and sediment. High-quality surf zone turbulence measurements are critical to diagnosing surf zone turbulence energetics. Measurements of the turbulent dissipation rate $\epsilon$, often used to study oceanic turbulence (e.g., Terray et al. 1996; Gerbi et al. 2009), are sparse within the surf zone. Measuring surf zone turbulence is challenging because breaking waves and strong currents exert powerful forces on instruments, the water and seabed both vary substantially, and the high levels of surf zone turbulence, bubbles, and suspended sediment (relative to other ocean environments) can corrupt velocity measurements.

Acoustic Doppler velocimeters (ADVs) measure three components of velocity at sampling rates between 2 and 25 Hz by measuring the Doppler shift of returned acoustic pulses (SonTek 2004). ADVs have been used to study waves (e.g., Thomson et al. 2007) and mean circulation (e.g., Apotsos et al. 2008) in the surf zone and nearshore. The ADV accurately measures Reynolds stress and turbulent velocity spectra in laboratory flumes (Voulgaris and Trowbridge 2001). ADVs have also been used to study turbulence in a laboratory surf zone (e.g., Scott et al. 2005), in estuarine and coastal (e.g., Kim et al. 2000) environments, and in the field surf (Bryan et al. 2003) and swash zone (Raubenheimber et al. 2004).

The ADV sensor also returns the backscattered acoustic signal strength (SS) and the correlation (CORR) of successive pings (e.g., Zedel et al. 1996). Both SS and CORR are used to diagnose ADV data quality. Surf zone ADV velocity measurements can be noisy with significant amounts of bad data (Elgar et al. 2001). The signal strength depends upon the density of scatterers (e.g., Lohrmann et al. 1994). With insufficient scatterers, SS is low and the velocity signal is unreliable. Within the surf zone, there is generally no shortage of scatterers (e.g., bubbles and suspended sediment). Low SS also occurs when the ADV sensor is exposed out of the water (i.e.,

*Corresponding author address:* F. Feddersen, 9500 Gilman Dr., Scripps Institution of Oceanography, La Jolla, CA 92093-0209.
E-mail: falk@coast.ucsd.edu

DOI: 10.1175/2010JTECHO783.1

above water level) or when the scatterer density is so high that the acoustic signal is absorbed or scattered (e.g., Elgar et al. 2005). Along-beam correlation, the coherence between the Doppler shift observed with successive pings, is low (Cabrera et al. 1987) when scatterers leave the sampling volume between pings or when velocity fluctuates or is sheared within the sample volume (Lhermitte and Lemmin 1994). Low CORR leads to inaccurate velocity estimates (Zedel et al. 1996). Low CORR also occurs in the presence of a significant number of bubbles (Mori et al. 2007b) and when the ADV sensing volume is too close to the bed (Martin et al. 2002; Elgar et al. 2005), that is, generally one sample volume width above the bed (Raubenheimber et al. 2004).

Elgar et al. (2005) suggest flagging data points as ''bad'' when the signal strength SS $< \gamma_{\mathrm{SS}}$ (SS is an eight-bit count: 0–255) from any of the three SonTek Ocean ADV acoustic beams. The signal strength cutoff $\gamma_{\mathrm{SS}} =$ 100 count was chosen by examination of surf zone data during times when the probe was known to be both in and out of the water. This $\gamma_{\mathrm{SS}}$ is specific to the particular SonTek ADV sensor, and other sensors may give different $\gamma_{\mathrm{SS}}$ (B. Raubenheimer 2009, personal communication). Elgar et al. (2005) reject an entire data run if the fraction of bad SS data points $\delta_{\mathrm{SS}} > 0.008$. This empirical criterion is conservative, assuring that little bad data passes.

The ADV correlation signal (ranging from 0 to 1.0) is also used to diagnose data quality (Zedel et al. 1996; SonTek 2004). To mark data points as bad, Elgar et al. (2005) proposed a correlation threshold $\gamma_{\mathrm{CORR}}$ of

$$\gamma_{\mathrm{CORR}} = 0.3 + 0.4\sqrt{f_s/f_{\max}}, \tag{1}$$

where $f_s$ is the sample frequency and $f_{\max}$ is the maximum ADV sampling frequency ($f_{\max} = 25$ Hz for the SonTek Ocean ADV). The upper (0.7) and lower (0.3) $\gamma_{\mathrm{CORR}}$ limits are based on SonTek (2004) estimates for full sampling and mean flow, respectively. Data points where the correlation $\gamma_{\mathrm{CORR}}$ is on any of the three beams are marked bad. Unlike the $\delta_{\mathrm{SS}}$ rejection criteria, Elgar et al. (2005) did not propose a data run rejection criteria based upon the fraction of bad CORR points $\delta_{\mathrm{CORR}}$. Instead, two quality control (QC) tests, based upon the expected properties of the surface gravity wave field in the sea swell band, are used to reject data runs. The first test statistic is the pressure $p$ to (interpolated-) cross-shore velocity ($u$) coherence $\overline{\mathrm{C}}_{pu}$, and the second statistic is based upon the ratio of the pressure to horizontal velocity variance (i.e., $Z^2$, Guza and Thornton 1980). Thresholds for $Z^2$ and $\overline{\mathrm{C}}_{pu}$ tests were selected empirically. A large $\delta_{\mathrm{CORR}}$ usually indicated that a data run would not pass the $Z^2$ and $\overline{\mathrm{C}}_{pu}$ tests, but some cases with large $\delta_{\mathrm{CORR}}$ (up to $\delta_{\mathrm{CORR}} = 0.5$) did pass these tests (Elgar et al. 2005). This ADV QC methodology works well for wave and mean current studies (i.e., at frequencies $< 0.3$ Hz), but is constrained by the requirement of a collocated and synchronized pressure measurement.

Turbulent dissipation rate $\epsilon$ estimates depend crucially upon the high-frequency ($>$1 Hz) component of the velocity spectrum rather than on sea-swell band frequencies ($\sim$0.1 Hz). In nearshore and surf zone field studies of $\epsilon$, ADV QC methods vary. In 4.5-m mean water depth, a location only occasionally within the surf zone, ADV measurements 1 m above the bed were used to estimate $\epsilon$ (Trowbridge and Elgar 2001). ADV data quality control used the manufacturer's suggested $\gamma_{\mathrm{CORR}}$; $\delta_{\mathrm{CORR}}$ levels and bad data interpolation were not discussed. Instead, assuming unidirectional and pure shallow-water wave orbital motions with a steady current, Trowbridge and Elgar showed that within an inertial subrange (at high frequencies with no instrument noise)

$$\frac{(12/21)[P_{uu}(f) + P_{vv}(f)]}{P_{ww}(f)} = 1, \tag{2}$$

where $P_{uu}$, $P_{vv}$, and $P_{ww}$ are the cross-shore, alongshore, and vertical velocity spectra, respectively, and $f$ is frequency. The quality of $\epsilon$ estimates was ensured by checking that a ratio $R$, based upon the lhs of (2), was near 1. Although the assumptions used to derive (2) are not generally valid within a natural surf zone, on average, $R \approx 0.8$ was observed, suggesting that a turbulent inertial subrange was present and the resulting $\epsilon \lesssim 10^{-4}$ m$^2$ s$^{-3}$ (Trowbridge and Elgar 2001).

In a study of the $\epsilon$ vertical structure seaward of the surf zone (no depth-limited wave breaking) in 3.5-m mean water depth (Feddersen et al. 2007), the SS and CORR (1) thresholds (Elgar et al. 2005) were applied to data from a vertical stack of three ADVs. No collocated pressure sensor was present, and thus the $Z^2$ and $\overline{\mathrm{C}}_{pu}$ tests (Elgar et al.) could not be applied. For all ADV data runs, the maximum $\delta_{\mathrm{CORR}} = 0.026$, and $\delta_{\mathrm{CORR}}$ was typically much less. Data flagged as bad were interpolated following Elgar et al. (2005), and the resulting $R$ varied between 0.8 and 1.5, and $\epsilon$ varied between $10^{-5}$ and $3 \times 10^{-4}$ m$^2$ s$^{-3}$. However, these observations did not reach far up in the water column as $z'/H_{\mathrm{sig}} \geq 1$ ($z'$ is the ADV distance below the mean sea surface and $H_{\mathrm{sig}}$ is the significant wave height).

In an study of turbulent energetics with whitecapping wave breaking in 16-m water depth (Gerbi et al. 2009), data runs with large vertical velocities or ADV sensors too close to the surface (i.e., $z'/H_{\mathrm{sig}} < 2$) were rejected, and the resulting $\epsilon \lesssim 10^{-5}$ m$^2$ s$^{-3}$. In a shallow estuary (1.5–3.5-m depth) study (Jones and Monismith 2008) of the $\epsilon$ vertical structure with whitecapping wind waves ($H_{\rm sig}$ between 0.1 and 0.6 m), the ADV velocity QC methods were not specified. Estimates of $\epsilon$ were rejected if the vertical velocity spectrum was not consistent with a $-5/3$ power law over some frequency range. Measurements were reported relatively high up in the water column with $z'/H_{\rm sig}$ as small as 0.3 and $z/h$ (where $z$ is height above the bed and $h$ is the mean water depth) as large as 0.9. The resulting $\epsilon$ was generally $\lesssim 10^{-4}$ m$^2$ s$^{-3}$, but occasionally as large as $10^{-3}$ m$^2$ s$^{-3}$ high up in the water column.

In a study of surf zone $\epsilon$ in <3 m depths and with incident $H_{\rm sig} < 0.6$ m (Bryan et al. 2003), SonTek Ocean ADV data points with SS and CORR below $\gamma_{\rm SS} = 77$ counts and $\gamma_{\rm CORR} = 0.7$ were marked as bad. Data runs were rejected if the fraction of total bad data points > 0.1, resulting in 62 of the 194 data runs being discarded. The data interpolation method was not specified. Data runs were additionally rejected if the best-fit velocity spectra power law was not near $-5/3$. The resulting $\epsilon$ varied between $10^{-5}$ and $10^{-3}$ m$^2$ s$^{-3}$. Some retained data runs were relatively high up in the water column, at time exceeding $z/h > 0.7$.

In a swash one turbulence study (Raubenheimber et al. 2004), two vertical stacks of (two-velocity component) ADVs were deployed in 5-cm and 25-cm mean water depth. At the 25-cm location, the ADV was considered submerged (from the SS signal) most (98%) of the time. At the 5-cm location, only 25% of the data runs were considered submerged. Bad data points were removed following Elgar et al. (2005). Data runs considered submerged rarely had $\delta_{\rm CORR} > 0.03$. Velocity spectra were calculated from the Fourier transform of the velocity autocovariance, precluding the need for data-gap interpolation, but perhaps biasing the spectra estimates. The turbulent dissipation rate $\epsilon$ was estimated from the high-frequency spectra following Trowbridge and Elgar (2001). The observed $\epsilon$ were the largest oceanic $\epsilon$ ever reported, up to $10^{-1}$ m$^2$ s$^{-3}$, and were an order of magnitude larger than the combined shear production and depth-normalized breaking wave energy flux gradient (Raubenheimber et al. 2004).

Here, surf zone and nearshore ADV data are used to examine and develop a quality control methodology for estimating surf zone $\epsilon$. This process also should be applicable to open ocean air–sea boundary $\epsilon$ studies. Note that this QC methodology is not appropriate for estimating other turbulent parameters, such as the Reynolds stress. The surf zone and nearshore field ADV observations from the Huntington Beach, California, fall 2006 (HB06) field experiment are described in section 2. Bad ADV velocity data points are identified (Elgar et al. 2005) with both the ADV signal strength and correlation signals (section 3). The fraction of bad-SS data points $\delta_{\rm SS}$ is a function of the (wave amplitude) normalized ADV transducer depth below the surface. The bad SS data gap statistics are used to assist in identifying a $\delta_{\rm SS}$ cutoff to reject bad SS data runs. The fraction of bad CORR points $\delta_{\rm CORR}$ can be large even with small $\delta_{\rm SS}$. The resulting $\delta_{\rm CORR}$ is related to both the sensing volume distance below the surface and the wave energy flux gradient, consistent with turbulence- and bubble-induced Doppler noise within the sensing volume.

The method for estimating $\epsilon$, the QC tests, and their application are described in section 4. The two QC tests are based upon the properties of the turbulent inertial subrange. Velocity spectra are calculated from "patched" and "interpolated" time series. At smaller $\delta_{\rm CORR}$ (<0.1), patching and interpolation give similar results. At higher $\delta_{\rm CORR}$, patched data runs are more often consistent with an inertial subrange, and some data runs pass with $\delta_{\rm CORR}$ as high as 0.4. The implications of the $\epsilon$ QC method are discussed in section 5. The interpolated $\epsilon$ estimates are biased low relative to patched $\epsilon$ estimates. Previous QC methods designed for wave studies are shown to be inappropriate for $\bar{\epsilon}$ QC. Surf zone $\epsilon$ estimates can be consistently made at about 1.5 × wave amplitude below the mean sea surface, corresponding to the lower 60% of the water column in a saturated surf zone. The results are summarized in section 6.

## 2. The HB06 surf zone ADV observations

### *a. HB06 instrumentation and processing*

Surf zone field observations were collected during fall 2006 at Huntington Beach State Park (33.636°N, −117.969°E) as part of the HB06 experiment (Spydell et al. 2009; Clark et al. 2010; Omand et al. 2010, manuscript submitted to *Limnol. Oceanogr.*). A cross-shore transect of six instrumented frames was deployed spanning 160 m from near the shoreline out to 4-m mean water depth (Fig. 1). An additional deployed instrumented frame (between instruments 1 and 2) was often buried, and observations from it are not included here. At each instrument location, the vertical coordinate $z$ is positive upward with $z = 0$ m at the bed. The cross-shore coordinate $x$ is positive offshore. The instrument frames were leveled with possible orientation errors of ±3°. The tide range was approximately ±1 m. Data were collected for 800 h from 14 September to 17 October 2006.

Each instrumented frame had a buried pressure ($p$) sensor and a mounted downward-looking 5-MHz SonTek Ocean Probe ADV (SonTek 2004) with synchronized data collection sampled at 8 Hz. Vertical instrument locations were GPS measured to within a few centimeters

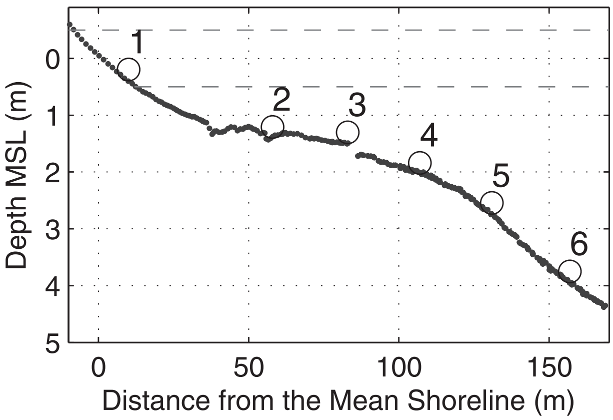


FIG. 1. HB06 cross-shore depth transect vs distance from the mean shoreline The instrumented frame locations are given by the circles and numbered 1–6. An additional instrumented frame, located between 1 and 2, was often buried, and is not considered here. The typical tide range is shown with the horizontal dashed lines.

relative to mean sea level. The ADV measures three components of velocity ($u$, $v$, and $w$) aligned with the coordinate system. The velocity range was set to $\pm 5$ m s$^{-1}$ and velocities beyond this range (i.e., phase wrapping) were not observed. In addition, the ADV returns signal strength and correlation on each of the three beams. Both SS and CORR are given as an unsigned byte (0–255 counts) and CORR is normalized to between 0 and 1.0. In each hourly data run, the ADV sampled 24 578 data points (51.2 min or 3072 s) and subsequently went into bottom-finding mode for the remainder of the hour to estimate ADV transducer height above the seabed ($z_{\mathrm{tr}}$) and bed location (relative to mean sea level).

From each pressure sensor, the mean sea surface location, mean water depth $h$, and sea surface elevation spectra ($P_{\eta\eta}$) were estimated hourly. These calculations are independent of the collocated ADV velocity data. Pressure spectra from buried sensors were adjusted following Raubenheimber et al. (1998). From the spectra, significant wave height $H_{\mathrm{sig}}$ is calculated over both swell (0.03–0.3 Hz, $H_{\mathrm{sig}}^{\mathrm{ss}}$) and infragravity (0.003–0.03 Hz, $H_{\mathrm{sig}}^{\mathrm{ss}}$) frequency bands. The total (sea swell and infragravity bands) significant wave amplitude $a_{\mathrm{sig}}$ is given by $a_{\mathrm{sig}} = [(H_{\mathrm{sig}}^{\mathrm{ss}})^2 + (H_{\mathrm{sig}}^{\mathrm{ss}})^2]^{1/2}/2$. During the experiment, the incident $H_{\mathrm{sig}}^{\mathrm{ss}}$ varied between 0.5 and 1.4 m.

The (downward looking) ADV sensing volume vertical location $z_{\mathrm{adv}}$ is 0.18 m below the transducer location $z_{\mathrm{tr}}$ (i.e., $z_{\mathrm{tr}} = z_{\mathrm{adv}} + 0.18$ m). The ADV sensing volume is a approximately (0.01 m)$^3$ cylinder (SonTek 2004). During the deployment the seabed eroded and accreted, and the ADVs were occasionally raised or lowered on the frames. At instruments 1–3, $z_{\mathrm{adv}}$ varied between 0 and 0.4 m, and at instruments 4–6, $z_{\mathrm{adv}}$ varied between 0.5 and 0.8 m. Data runs with sensing volume too close to the bed ($z_{\mathrm{adv}} \leq 0.03$ m) are rejected. The distance below the mean sea surface of the sensing volume $z'_{\mathrm{adv}}$ and transducer ($z'_{\mathrm{tr}}$) is given by $z'_{\mathrm{adv}} = h - z_{\mathrm{adv}}$ and $z'_{\mathrm{tr}} = h - z_{\mathrm{tr}}$, respectively. Both $z'_{\mathrm{adv}}$ and $z'_{\mathrm{tr}}$ are relevant because, when the transducer of a downward-looking ADV is exposed out of the water, the acoustic path is blocked even if the sensing volume remains submerged. For an upward-looking ADV this is not a concern as the sensing volume location would be exposed first. For a horizontally mounted ADV $z_{\mathrm{tr}} = z_{\mathrm{adv}}$.

## b. *Example of ADV data*

The challenges in using surf zone ADV data to estimate (high frequency) turbulence parameters are illustrated with a short (160 s) time series of ADV data (Fig. 2). In general, the vertical velocities are small ($|w| < 0.1$ m s$^{-1}$; Fig. 2a) as expected for shallow water surface gravity waves. The signal strength is typically SS $>$ 180 counts (Fig. 2b), well above the suggested $\gamma_{\mathrm{SS}} = 100$ counts cutoff (Elgar et al. 2005). In addition, correlations generally are high ($>$0.8; Fig. 2c) above the $\gamma_{\mathrm{CORR}} = 0.526$ [Eq. (1) with $f_s = 8$ Hz] cutoff (Elgar et al. 2001). However, occasionally the vertical velocities are large with large accelerations (e.g., $|w| > 0.8$ m s$^{-1}$ near $t = 150$ s in Fig. 2a) or noisy (e.g., near 35 s in Fig. 2a) when SS (Fig. 2b) or CORR (Fig. 2c) are low, falling below the suggested $\gamma_{\mathrm{SS}}$ and $\gamma_{\mathrm{CORR}}$ cutoffs. The SS has a minima at an apparent noise floor of 42 counts. CORR can fall below $\gamma_{\mathrm{CORR}} = 0.526$ when SS does not (i.e., near 20 s in Fig. 2). For the entire data run, $\delta_{\mathrm{SS}} = 0.016$, exceeding the Elgar et al. (2005) $\delta_{\mathrm{SS}} = 0.008$ cutoff, which would result in rejection of this data run. The fraction of combined bad SS and CORR data points $\delta_{\mathrm{CORR}} = 0.045$, exceeding that typically observed by Raubenheimber et al. (2004) and Feddersen et al. (2007). It is not known whether this level of $\delta_{\mathrm{CORR}}$ can be tolerated in estimating $\epsilon$.

# 3. QC of ADV data

## a. *SS QC of surf zone ADV data*

Within a data run, ADV data is marked bad when the returned signal strength SS $< \gamma_{\mathrm{SS}}$ at any of the three acoustic beams with $\gamma_{\mathrm{SS}} = 100$ counts (Elgar et al. 2005). With a ~42 count ADV noise floor (see Fig. 2b) and a 0.43 dB per count conversion, a $\gamma_{\mathrm{SS}} = 100$ count cutoff corresponds to a 25-dB cutoff, which is more conservative than the 15-dB SonTek (2004) recommendation. However, the resulting $\delta_{\mathrm{SS}}$ is insensitive to $\gamma_{\mathrm{SS}}$ within the range of 80–130 counts (16–38 dB).

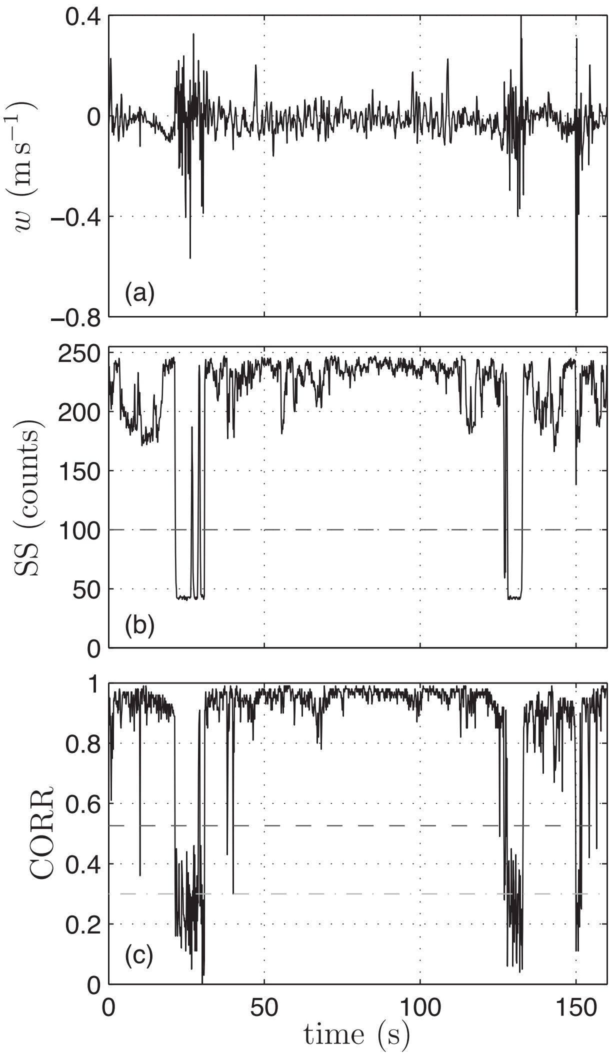


FIG. 2. Example ADV measured (a) vertical velocity $w$, (b) signal strength (SS), and (c) correlation (CORR) vs time. This 160-s-long data segment is from instrument 1 (see Fig. 1) at 0500 UTC 18 Sep. The dashed horizontal line in (b) is the suggested Elgar et al. (2005) $\gamma_{SS}$ cutoff. In (c) the correlation cutoffs (1) for $f_s$ = 8 Hz ($\gamma_{CORR}$ = 0.526, dashed) and the mean flow $f_s$ = 0 Hz ($\gamma_{CORR}$ = 0.3, dashed–dotted) are shown. The water depth $h$ = 0.57 m, $H_{sig}$ = 0.30 m, $z_{adv}$ = 0.13 m, and $z_{tr}$ = 0.26 m.

The fraction of bad SS data runs $\delta_{SS}$ is calculated for all data runs. At all instruments, $\delta_{SS}$ did not systematically depend upon instrument height above the bed, indicating that high levels of near-bed suspended sediment (e.g., Beach and Sternberg 1996) does not adversely impact ADV signal strength. In the nearshore and surf zone, the sea surface fluctuates owing to infragravity and sea swell surface gravity waves that can expose out of the water an instrument deployed below the mean surface. The amount that the ADV transducer is exposed out of the water, and thus $\delta_{SS}$, is expected to increase with smaller $z'_{tr}$ (the distance of the downward-facing ADV transducer below the mean sea surface) and increase with larger significant wave amplitude $a_{sig}$. Reflecting this, $\delta_{SS}$ is inversely related to the normalized ADV transducer depth $z'_{tr}/a_{sig}$ (Fig. 3) with a consistent relationship that collapses at all surf zone instrument locations (1–4). At $z'_{tr}/a_{sig}$ = 0.5, $\delta_{SS}$ generally varies between 0.1 and 0.2, and for larger $z'_{tr}/a_{sig} \geq 1$ (conceptually, the ADV transducer below the significant trough level), $\delta_{SS}$ is much reduced, generally <0.02. At the mean sea surface ($z'_{tr}/a_{sig} = 0$), $\delta_{SS} \approx 0.5$, consistent with an exposed transducer face 50% of the time. If $a_{sig}$ does not include infragravity fluctuations, the relationship between $\delta_{SS}$ and $z'_{tr}/a_{sig}$ does not collapse as well, particularly near the shoreline (instrument 1) where infragravity energy can be significant (e.g., Guza and Thornton 1985). At times (<2% of data runs), $\delta_{SS} > 0.01$ at instruments 5 and 6, which are always well below the mean surface ($z'_{tr}/a_{sig}$ > 1.75, 2.75, respectively; not shown). Other mechanisms (lack of sufficient scatterers or acoustic absorption/scattering) induce these moderate $\delta_{SS}$. The Elgar et al. (2005) $\delta_{SS} < 0.008$ criteria (horizontal dashed red line in Fig. 3) rejects all data runs with $z'_{tr}/a_{sig} \lesssim 1$, which may be of particular interest for turbulence studies.

The lower boundary of the $\delta_{SS} - z'_{tr}/a_{sig}$ relationship is approximately given by

$$\log_{10}(\delta_{SS}) = -0.3(z'_{tr}/a_{sig} + c)^4 - 1.2(z'_{tr}/a_{sig} + c)^2 - 0.3, \tag{3}$$

where $c$ = 0.15 (gray-dashed curve in Fig. 3). Although not aesthetically pleasing, the relationship (3) holds at all surf zone instruments regardless of whether in the swash zone (lower tide at instrument 1) or surf zone. When designing surf zone ADV deployments, (3) yields a $\delta_{SS}$ estimate for a downward-facing ADV. For example, if $\delta_{SS}$ = 0.1 is tolerable, then measurements potentially can be made as shallow as $z'_{tr}/a_{sig} \approx 0.5$.

For each data run, the bad SS data gaps are binned into probability density functions (pdfs) of data gap lengths from 1/8 to 60 s. The data-gap-length statistics dependence upon $\delta_{SS}$ is used to help determine criteria to reject data runs. The pdf maximum (the mode) is typically at or near 1/8 s (one sample) for all $\delta_{SS}$ (blue dots in Fig. 4). The gap length means and standard deviations (std dev) increase with increasing $\delta_{SS}$ (circles and asterisks in Fig. 4). At all $\delta_{SS}$, the data gap length means and std dev are roughly equal, and together with a one-point mode, suggest approximately exponentially distributed data gap lengths. The data-gap-length statistics dependence upon $\delta_{SS}$ is independent of ADV

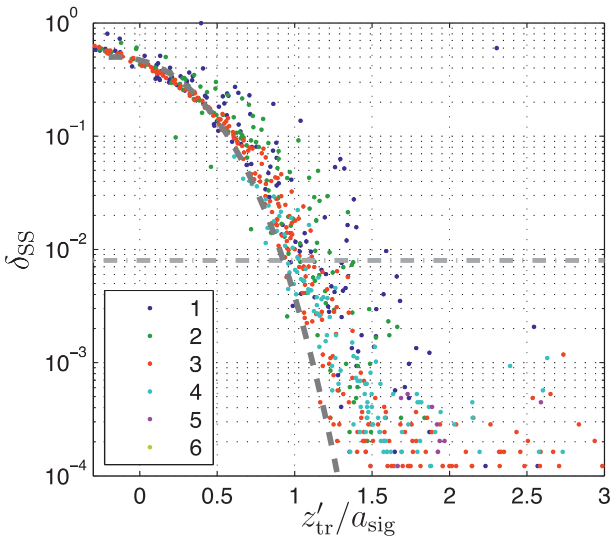


FIG. 3. Fraction of bad SS data points $\delta_{SS}$ vs $z'_{tr}/a_{sig}$ at instruments 1–6 (see legend), where is $z'_{tr}$ the distance of the ADV transducer below the mean sea surface and $a_{sig}$ is the significant wave amplitude. Note that no instrument 6 data points are present in this axes range. The horizontal dashed–dotted line is the $\delta_{SS} = 8 \times 10^{-3}$ cutoff for discarding a data run (Elgar et al. 2005). The black-dashed curve is the proposed scaling (3) based upon the data.

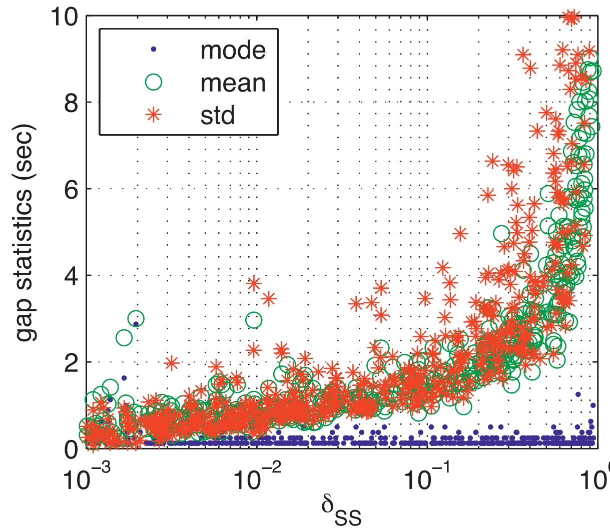


FIG. 4. Mode, mean, and standard deviation of bad SS gap lengths vs $\delta_{SS}$ at all instruments.

location. For $\delta_{SS} \le 0.1$, both data gap length mean and std dev are typically <2 s and are linear with $\log_{10}(\delta_{SS})$. For example, between the order of magnitude change from $\delta_{SS} = 10^{-2}$ to $\delta_{SS} = 10^{-1}$, the data gap length mean and std dev only increase from ~1 to 2 s. For larger $\delta_{SS}$ (>0.1), the gap length means and std dev increase rapidly, suggesting a different nature of exposure out of the water and that such $\delta_{SS}$ levels are not tolerable.

Bad SS data runs consistently out of the water are rejected with a $\delta_{SS}$ cutoff $\delta^c_{SS}$ (i.e., data runs with $\delta_{SS} > \delta^c_{SS}$). A balance is sought in selecting $\delta^c_{SS}$ to retain data runs higher in the water column of interest for turbulence studies. At typical mid-surf-zone locations (2 and 3), varying $\delta^c_{SS}$ from 0.008 (e.g., Elgar et al. 2005) to 0.1 results in ⅓–½ more retained good-SS data runs with smaller $z'_{tr}/a_{sig}$. Since the bad-SS data gap statistics are still small and increasing slowly (Fig. 4), the SS cutoff $\delta^c_{SS} = 0.1$ is chosen to retain more of the surf zone data runs within the range $0.6 < z'_{tr}/a_{sig} < 1.5$ (Fig. 3) that would otherwise be rejected. The impact of this choice is subsequently discussed.

### b. *Correlation QC of surf zone ADV data*

After rejecting bad SS ($\delta_{SS} > 0.1$) data runs, the correlation QC is applied to the remaining data runs. Data points with CORR < $\gamma_{CORR}$ on any of the three ADV beams are marked as bad, where $\gamma_{CORR} = 0.562$ is given by (1) with $f_s = 8$ Hz (Elgar et al. 2005). Bad SS data points are also marked as bad CORR. The resulting fraction of total bad data points, denoted $\delta_{CORR}$, can be significantly larger than $\delta_{SS}$ (Fig. 5). Even for small $\delta_{SS}$ (<$10^{-3}$), $\delta_{CORR}$ can approach one, reflecting the different processes leading to low signal strength (exposure out of the water) and low correlation (Doppler noise or bubbles). Instruments 2, 3, and 4, with the strongest levels of wave breaking, consistently have the largest values of $\delta_{CORR}$ relative to $\delta_{SS}$ (see legend in Fig. 5). An alternative velocity QC algorithm (i.e., despiking; Goring and Nikora 2002), which uses velocity signal properties together with a minimum CORR of 0.3, generally gives a similar fraction bad data points as $\delta_{CORR}$ (see the appendix).

For examining $\delta_{CORR}$ dependencies, the sensing volume vertical location ($z_{adv}$ or $z'_{adv}$), as opposed to $z_{tr}$, is the appropriate vertical location as Doppler noise within the sensing volume leads to low correlations (e.g., Lhermitte and Lemmin 1994). The $\delta_{CORR}$ do not depend systematically upon elevation of the sensing volume above the bed ($z_{adv}$). Wave breaking is a source of surf zone turbulence (George et al. 1994; Bryan et al. 2003; Feddersen and Trowbridge 2005) and bubbles (e.g., Deane and Stokes 2002) to the upper water column. Thus, elevated $\delta_{CORR}$ are expected higher up in the water column and under more intense breaking waves. The breaking wave turbulence and bubble input rate depends upon the wave energy flux gradient $dF/dx$, where $F$ is the cross-shore wave energy flux. The $\delta_{CORR}$ relationship to $z'_{adv}/a_{sig}$ and $dF/dx$ is examined.

Assuming nonreflective, normally incident waves and integrating over the sea swell band (0.05–0.3 Hz), the energy flux $F$ is estimated at each instrument location solely from pressure via

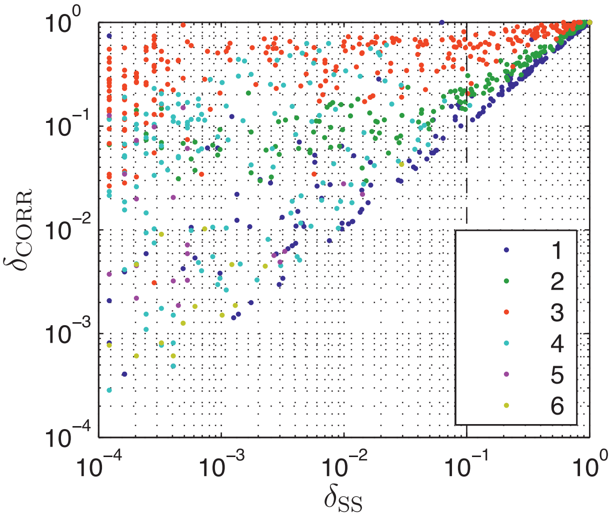


FIG. 5. Plot of $\delta_{\mathrm{CORR}}$ vs $\delta_{\mathrm{SS}}$ at all instruments (see legend). The vertical dashed line indicates the $\delta_{\mathrm{SS}} = 0.1$ cutoff.

$$F = g\int_{0.05\mathrm{Hz}}^{0.3\mathrm{Hz}} P_{\eta\eta}(f)c_g(f)\,df, \tag{4}$$

where $g$ is the gravitation constant and $c_g$ is the linear-theory group velocity. These wave energy flux estimates (4) are largely consistent with estimates derived from combined pressure + ADV data that take into account nonnormal wave incidence and reflection (Sheremet et al. 2005). However, the (pressure + ADV)-based $F$ estimates are not independent of ADV data quality and thus are not used. Wave energy flux gradients d$F$/d$x$ are estimated at instruments 1–5 by differencing $F$ estimates from the neighboring onshore and offshore instruments. At location 1, $F = 0$ is assumed at the shoreline.

Considering only good-SS data runs, the relationship of $\delta_{\mathrm{CORR}}$ to $z'_{\mathrm{adv}}/a_{\mathrm{sig}}$ (Fig. 6a) is analogous to that for $\delta_{\mathrm{SS}}$ (Fig. 3) with $\delta_{\mathrm{CORR}}$ increasing with smaller $z'_{\mathrm{adv}}/a_{\mathrm{sig}}$. In contrast to the tighter $\delta_{\mathrm{SS}}$ relationship, the $\delta_{\mathrm{CORR}}$ range increases with $z'_{\mathrm{adv}}/a_{\mathrm{sig}}$. As $z'_{\mathrm{adv}}/a_{\mathrm{sig}} \to 1$, the data cloud becomes a nose and $\delta_{\mathrm{CORR}} \to 1$ (Fig. 6b). For any data runs with $z'_{\mathrm{adv}}/a_{\mathrm{sig}} \leq 1$, $\delta_{\mathrm{CORR}} > 0.7$ (not shown). Note that the nondimensional instrument depths $z'_{\mathrm{adv}}/a_{\mathrm{sig}}$ are larger than $z'_{\mathrm{adv}}/a_{\mathrm{sig}}$ (Fig. 3) and are not directly comparable.

At fixed $z'_{\mathrm{adv}}/a_{\mathrm{sig}}$ $\delta_{\mathrm{CORR}}$ is generally larger with increasing $dF/dx$ (note the color stratification in Fig. 6), particularly for $1 < z'_{\mathrm{adv}}/a_{\mathrm{sig}} < 2.5$ (Fig. 6b). Nondimensionalized surf zone dissipation observations (e.g., George et al. 1994) and bubbles (e.g., Garret et al. 2000) decay with depth. The elevated $\delta_{\mathrm{CORR}}$ closer to the surface and with stronger wave breaking is consistent with small-scale turbulent- or bubble-induced Doppler noise within the sensing volume. Measurements closer to the bed (e.g., $z'_{\mathrm{adv}}/a_{\mathrm{sig}} = 3$), even with large $dF/dx$ (red points in Fig. 6a), can have low $\delta_{\mathrm{CORR}}$ ($<10^{-3}$) as small-scale turbulence and bubbles are reduced farther below the surface. With the factors that affect $\delta_{\mathrm{CORR}}$ known, the dependence of the $\epsilon$ QC upon $\delta_{\mathrm{CORR}}$ is examined next.

## 4. Quality control of turbulent dissipation rate $\epsilon$

### a. Calculation of $\epsilon$

Turbulent dissipation rate $\epsilon$ is estimated from the observed (high) frequency vertical velocity spectrum with the Lumley and Terray (1983) model that converts a wavenumber ($k$) spectrum $\hat{P}_{ww}(k)$ to a frequency spectrum $P_{ww}(f)$ for frozen turbulence in a mixed wave and mean current environment. Variants of this method have been used to estimate nearshore $\epsilon$ (Trowbridge and Elgar 2001; Bryan et al. 2003; Feddersen et al. 2007). A Kolmogoroff inertial subrange velocity wavenumber spectra $\hat{P}_{ww}(k) \sim \epsilon^{2/3}k^{-5/3}$ due to homogeneous isotropic turbulence (e.g., Batchelor 1953) is assumed present. At frequencies higher than the sea swell frequencies (i.e., >1 Hz), $\epsilon$ is derived from the observable $P_{ww}(f)$ through the model form (Lumley and Terray 1983; Trowbridge and Elgar 2001)

$$P_{ww}(f) = \frac{\alpha\epsilon^{2/3}}{2(2\pi)^{3/2}} M_{ww}(f; \overline{\mathbf{u}}, \sigma^2_{u,v,w}), \tag{5}$$

where $\alpha = 1.5$ is the Kolmogoroff constant, $\overline{\mathbf{u}}$ and $\sigma^2_{u,v,w}$ are the mean and (wave dominated) variance of the three velocity components, and $M_{ww}$ is an integral over 3D wavenumber space that transforms the inertial subrange $k^{-5/3}$ wavenumber dependence to frequency (Trowbridge and Elgar 2001; Feddersen et al. 2007). For a nonzero velocity mean and variance, $M_{ww} \sim f^{-5/3}$ (Gerbi et al. 2009), meaning that, within an inertial subrange, $P_{ww}(f) \sim f^{-5/3}$. Because noise levels are lower for the flow component parallel to the ADV orientation, the vertical (parallel to ADV body) velocity spectrum $P_{ww}(f)$ is used to estimate $\epsilon$. Given the observed $P_{ww}(f)$ and estimated $M_{ww}$, the estimated $\epsilon(f)$ are calculated via (5).

Once bad SS and CORR data points are flagged, gap-free time series are generated in two ways to calculate velocity spectra. The first is "interpolation," following Elgar et al. (2005), resulting in a time series denoted by $w^{(\mathrm{i})}$. Data gaps ≤1-s long (eight data points) are linearly interpolated from the good data points bounding the gap. Bad data within the longer gaps is averaged together and the entire gap is set to this constant average value. The rationale is that velocity data noise is unbiased (as long as instrument is in the water) so that averaging the

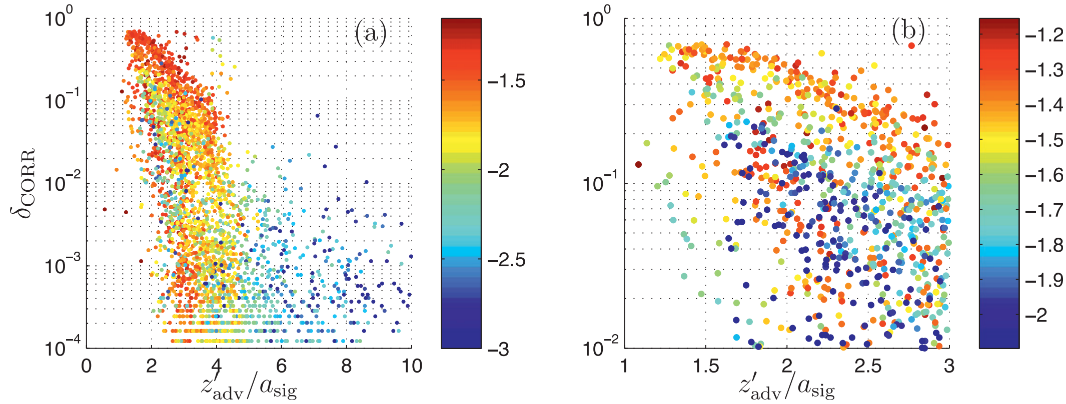


FIG. 6. (a) The $\delta_{\mathrm{CORR}}$ vs $z'_{\mathrm{adv}}/a_{\mathrm{sig}}$ at instruments 1–5 where $\log_{10}$ of the energy flux gradient $dF/dx$ ($\mathrm{m^3\ s^{-3}}$) is colored. Only good-SS data runs that satisfy the $\delta_{\mathrm{SS}} \le 0.1$ criteria are shown. Data runs with $\delta_{\mathrm{CORR}} > 0.7$ are not shown. (b) Close up of the nose regions in (a).

gap results in a more accurate mean current over the gap (Elgar et al. 2005). The interpolation method acts analogously to a low-pass filter biasing the high-frequency spectra low. The second method is "patching" (e.g., $w^{(\mathrm{p})}$), which combines linear interpolation of short data gaps ($\le$0.5 s or four data points) and "patching together" longer data gaps. Patching is illustrated with a discrete data sequence

$$w_k, w_{k+1}, w_{k+2}, \ldots, w_{k+m}, w_{k+m+1},$$

with a bad data gap of length $m$ from indices $k + 1$ to $k + m$. Patching cuts out the data from the gap and joins the good ends so that $w_{k+m+1} \rightarrow w_{k+1}$, reducing the time series length by the total number of bad data points. Patching has the potential for creating large steps in the resulting $w^{(p)}$ time series where the data gap ends are joined, which is expected to enhance (bias high) the high-frequency spectrum. The interpolation of the shorter (and by far most common) gaps reduces the amount of time shifting, which would otherwise redistribute the spectrum's frequency distribution. Quantities (i.e., spectra $\epsilon$) derived from patched and interpolated time series are denoted with (p) and (i) superscripts, respectively. Both patched and interpolated quantities are denoted with superscript (p, i).

Velocity spectra [$P^{(\mathrm{p,i})}_{uu}(f)$, $P^{(\mathrm{p,i})}_{vv}(f)$, and $P^{(\mathrm{p,i})}_{ww}(f)$] are calculated from the patched and interpolated time series using 70-s-long data segments (detrended and Hanning windowed with 50% overlap), resulting in 88 degrees of freedom. At any frequency, the true spectrum is 95% likely to be found within a factor of [0.76, 1.38] of the observed spectrum. Analogously, $M^{(\mathrm{p,i})}_{ww}(f; \overline{\mathbf{u}}, \sigma^2_{u,v,w})$ is estimated (see Feddersen et al. 2007) with the velocity mean and variance from the appropriate time series. Both $P^{(\mathrm{p,i})}_{ww}$ and $M^{(\mathrm{p,i})}_{ww}$ are only calculated for good-SS (i.e., $\delta_{\mathrm{SS}} \le 0.1$) data runs that also pass the very broad criterion that $\delta_{\mathrm{CORR}} \le 0.7$.

Both patched [$\epsilon^{(\mathrm{p})}(f)$] and interpolated [$\epsilon^{(\mathrm{i})}(f)$] dissipation are estimated at $N_f = 56$ frequencies between 1.2 and 2 Hz via

$$\epsilon^{(\mathrm{p,i})}(f) = \left[\frac{P^{(\mathrm{p,i})}_{ww}(f)2(2\pi)^{3/2}}{\alpha M^{(\mathrm{p,i})}_{ww}(f; \overline{\mathbf{u}}, \sigma^2_{u,v,w})}\right]^{3/2}. \tag{6}$$

This frequency range has been used previously (e.g., Trowbridge and Elgar 2001; Feddersen et al. 2007) since little surface gravity wave variance is assumed present at these frequencies. Consistent with this assumption, a slope break is often observed in velocity spectra [e.g., near $f = 0.5$ Hz, Smyth and Hay (2003)]. If the model and inertial subrange wavenumber spectrum are correct, then $\epsilon(f)$ should be constant with $f$. At higher frequencies (>3 Hz), $P_{ww}$ generally has an approximately constant noise floor. Assuming no $M_{ww}$ error induced by $\overline{\mathbf{u}}$ or $\sigma^2_{u,v,w}$ error, the $P_{ww}$ spectra error bars result in the true $\epsilon^{(\mathrm{p,i})}(f)$ found within the interval [0.66, 1.61] of the observed $\epsilon^{(\mathrm{p,i})}(f)$. Mean (frequency averaged) dissipation rate $\overline{\epsilon}^{(\mathrm{p,i})}$ for the data run is calculated by averaging $\epsilon^{(\mathrm{p,i})}(f)$ over all frequencies. Alternative averaging methods, that is, $\overline{\epsilon} = \exp[\langle \log \epsilon(f) \rangle]$ (Feddersen et al. 2007), result in a negligible difference (typically 1%, always <5%) to standard averaging. The $\overline{\epsilon}$ standard error $\varepsilon_{\overline{\epsilon}}$ is estimated from the variance of $\epsilon(f)$, that is, $\varepsilon^2_{\overline{\epsilon}} = \mathrm{var}[\epsilon(f)]/(N_f - 1)$. (Note that the symbol $\varepsilon$ is used to represent standard errors where the symbol $\epsilon$ is used to represent dissipation rate.)

The resulting dissipation estimates $\overline{\epsilon}^{(\mathrm{p})}$ (and $\overline{\epsilon}^{(\mathrm{i})}$) range between $10^{-6}\ \mathrm{m^2\ s^{-3}}$ and $3 \times 10^{-3}\ \mathrm{m^2\ s^{-3}}$ and increase with $\delta_{\mathrm{CORR}}$ (Fig. 7). Although the ratio $\varepsilon_{\overline{\epsilon}^{(\mathrm{p})}}/\overline{\epsilon}^{(\mathrm{p})}$ (varying between 0.03 and 0.06) is small, the $\overline{\epsilon}$ standard error does

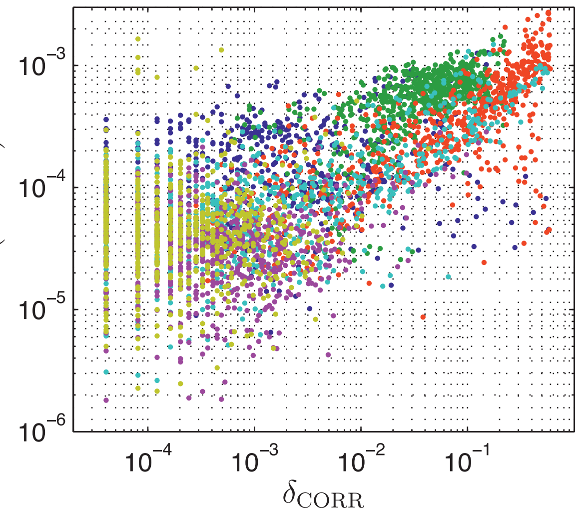


FIG. 7. Plot of $\overline{\epsilon}^{(p)}$ vs $\delta_{CORR}$ for good-SS data runs at all instruments (see legend in Fig. 5).

not indicate whether a data run $\overline{\epsilon}$ is consistent with an inertial subrange. The $\overline{\epsilon}^{(p,i)}$ increase with $\delta_{CORR}$ may be natural because the more turbulent the surf zone, the larger $\epsilon$ and also the larger $\delta_{CORR}$. However, it is not a priori clear whether $\overline{\epsilon}$ estimates at a particular $\delta_{CORR}$ are valid and what $\delta_{CORR}$ level quality $\overline{\epsilon}$ estimates can be obtained. Additional quality control tests are applied to reject data runs inconsistent with an expected inertial subrange.

### b. *Example of $P_{ww}$ and $\epsilon(f)$ frequency variability*

Examples of "interpolated" velocity spectra, for example, $P_{ww}^{(i)}(f)$, and frequency-dependent dissipation, $\epsilon^{(i)}(f)$, from two data runs at instrument 3 (with the most intense wave breaking and strongest currents) are shown in Fig. 8. In the first example (Fig. 8a), $\delta_{CORR} = 0.028$ is moderate and $H_{sig}/h = 0.45$, indicative of the outer surf zone, with observations relatively far ($z'_{adv}/a_{sig} = 3.32$) from the surface. The horizontal velocity spectra $P_{uu}^{(i)} + P_{vv}^{(i)}$ has a surface gravity wave peak (at $f = 0.07$ Hz) that falls off rapidly at intermediate frequencies, $0.3 < f < 0.7$ Hz, before encountering a slope break at $f = 0.8$ Hz (red curve in Fig. 8a). At higher frequencies (0.8–3 Hz), $P_{ww}^{(i)}$ follows a power law with (between 1.2 and 2 Hz) best-fit exponent, $\mu^{(i)}(\pm\varepsilon_{\mu}^{(i)}) = -1.74$ ($\pm 0.12$, where $\varepsilon_{\mu}^{(i)}$ is the standard error of $\mu^{(i)}$), close to the theoretical Kolmogoroff $\mu = -5/3$ inertial subrange value (cf. dashed green to thin blue curves in Fig. 8a). Consistent with the best-fit $\mu^{(i)}$ near $-5/3$, the estimated $\epsilon^{(i)}(f)$ are relatively constant in frequency (black curve in Fig. 8c). The mean dissipation $\overline{\epsilon}^{(i)} = 1.03 \times 10^{-4}$ m$^2$ s$^{-3}$ (blue dashed line in Fig. 8c) and the best-fit slope of $\epsilon^{(i)}(f)$ with $f$, $-9.0 \times 10^{-6}$ m$^2$ s$^{-3}$ Hz$_Z^{-1}$ (dotted line in Fig. 8c), is statistically indistinguishable from zero. The $\epsilon^{(i)}(f)$ 95% confidence limits (shaded-gray region in Fig. 8c) also encompasses the $\overline{\epsilon}^{(i)}$ more than 95% of the time. The patched spectrum $P_{ww}^{(p)}$, power-law exponent $\mu^{(p)} = 1.75 \pm 0.11$, $\epsilon^{(p)}(f)$ slope ($=-9.4 \times 10^{-6}$ m$^2$ s$^{-3}$ Hz$_Z^{-1}$), and $\overline{\epsilon}^{(p)} = 1.17 \times 10^{-4}$ m$^2$ s$^{-3}$ are close to the respective interpolated quantities. That $\mu^{(p,i)}$ are near $-5/3$ suggests the presence of an inertial subrange and a quality $\overline{\epsilon}$ estimate.

The second example has a larger $H_{sig}/h = 0.55$, indicative of the inner surf zone measurements closer to the surface ($z'_{adv}/a_{sig} = 2.17$) and larger $\delta_{CORR} = 0.255$ (Fig. 8b). Although the velocity spectra is consistent with pressure over the sea swell band (e.g., $\overline{C}_{pu} = 0.91$), at higher (1–3 Hz) frequencies, $P_{uu}^{(i)} + P_{vv}^{(i)}$ is not monotonic (red curve in Fig. 8b) and the $P_{ww}^{(i)}$ spectra fall off too rapidly with frequency (power slope of $\mu^{(i)} = -2.18 \pm 0.09$) for an inertial subrange (cf. blue to dashed-green curve in Fig. 8b). The patched $\mu^{(p)} = -2.13 \pm 0.13$ is similar to $\mu^{(i)}$. Consistent with $\mu^{(i)} \neq -5/3$, $\epsilon^{(i)}(f)$ is reduced with increasing frequency. The $\epsilon^{(i)}(f)$ best-fit slope, $-2.1 \times 10^{-4}$ m$^2$ s$^{-3}$ Hz$^{-1}$ (dotted line in Fig. 8d), is significantly different from zero. Note that the $\epsilon^{(i)}(f)$ error bars (shaded region in Fig. 8d) always encompass $\overline{\epsilon}^{(i)} = 4.28 \times 10^{-4}$ m$^2$ s$^{-3}$, indicating that this type of test to reject $\overline{\epsilon}$ estimates is insufficient. Furthermore, the patched and interpolated quantities are not consistent as $\overline{\epsilon}^{(p)}/\overline{\epsilon}^{(i)} = 1.82$, all together indicating that this data run is inconsistent with a turbulent inertial subrange and that this $\overline{\epsilon}$ estimate should be rejected.

### c. *Application of $\epsilon$ QC tests*

Two independent QC tests, based upon the expected presence of an turbulent inertial subrange, are applied to the patched and interpolated data runs and evaluated as a function of $\delta_{CORR}$. Data runs that do not pass both tests are considered inconsistent with a turbulent inertial subrange and their $\overline{\epsilon}$ estimates are rejected. First, the $P_{ww}(f)$ power-law exponent $\mu$ is tested for consistency with $-5/3$. Second, a ratio of horizontal-to-vertical velocity spectra is required to be near unity. These tests, examining the velocity spectra frequency variation and a bulk (frequency integrated) quantity, are examined separately.

#### 1) SPECTRA POWER-LAW EXPONENT CONSISTENT WITH AN INERTIAL SUBRANGE

For each data run, the (patched and interpolated) best-fit exponents $\mu^{(p,i)}$ (with error bars $\pm\varepsilon_{\mu}^{(p,i)}$) are estimated by a least squares fit of $\log(P_{ww}^{(p,i)})$ with $\log(f)$ over frequencies 1.2–2 Hz, as in the case examples (Fig. 8). Fitted standard error ($\varepsilon_{\mu}^{(p)}$ and $\varepsilon_{\mu}^{(i)}$) typically vary between 0.09 and 0.15. The estimated $\mu^{(p)}$ generally vary

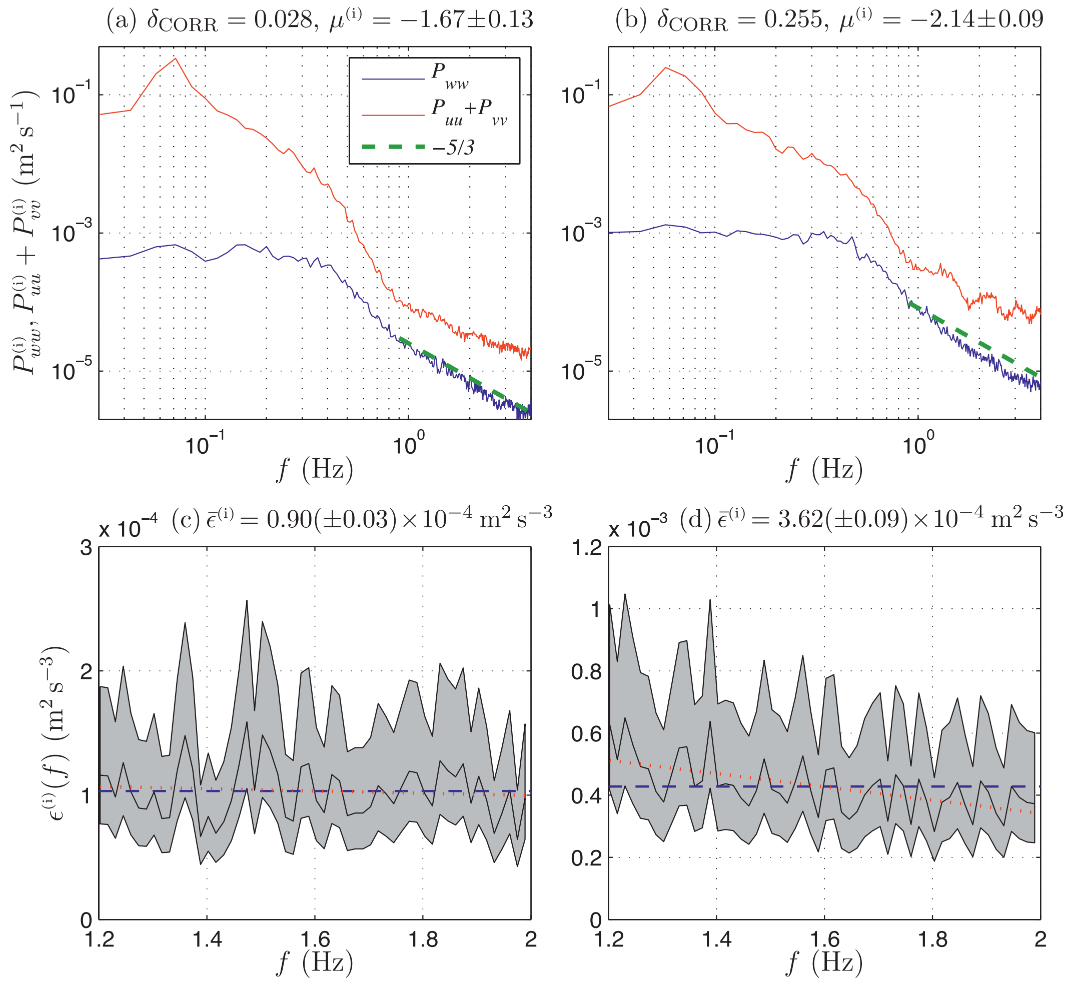


FIG. 8. Example of vertical velocity spectra $P^{(i)}_{ww}(f)$ vs frequency $f$ at instrument 3 that are (a) good (time = 240, $\delta_{\rm CORR} = 0.028$, $h = 1.83$ m, $H_{\rm sig} = 0.83$ m, $z'_{\rm adv}/a_{\rm sig} = 3.32$, and $\overline{C}_{pu} = 0.86$) and (b) bad (time = 280, $\delta_{\rm CORR} = 0.255$, $h = 1.03$ m, $H_{\rm sig} = 0.57$ m, $z'_{\rm adv}/a_{\rm sig} = 2.17$, and $\overline{C}_{pu} = 0.91$. A $-5/3$ power slope (green dashed line). (c),(d) Here $\epsilon^{(i)}(f)$ vs $f$ over a narrower frequency range that correspond to (a) and (b). Here $\epsilon^{(i)}(f)$ (black line), the error bars (shaded region, derived from $P^{(i)}_{ww}$), $\bar{\epsilon}^{(i)}$ (blue dashed line), and the linear best-fit slope (red dotted line).

between $-1$ and $-2.4$ (dots in Fig. 9a), although the range spans $[-4, 0]$. At all $\delta_{\rm CORR}$, the $\mu^{(p)}$ binned means are close to $-5/3$ (diamonds in Fig. 9a), suggesting that often an inertial subrange is present and that the Lumley and Terray (1983) model for converting wavenumber to frequency spectra often is applicable at all $\delta_{\rm CORR}$ levels. The $\mu^{(p)}$ binned std dev are generally near 0.35 and do not vary systematically with $\delta_{\rm CORR}$ (vertical lines in Fig. 9a). At $\delta_{\rm CORR} < 0.1$, the interpolated $\mu^{(i)}$ and patched $\mu^{(p)}$ are similar (Fig. 9b). At larger $\delta_{\rm CORR}$, the $\mu^{(i)}$ binned means are consistently $< -5/3$ and decrease with larger $\delta_{\rm CORR}$. These steeper spectral slopes are an artifact of the "interpolation" scheme, which at higher $\delta_{\rm CORR}$ increasingly reduces high-frequency energy (i.e., is a low-pass filter).

The consistency of the estimated $\mu^{(p)}$ and $\mu^{(i)}$ with $-5/3$, as expected in an inertial subrange in a wave–current environment (Gerbi et al. 2009), are tested to reject data runs. An analogous test examines whether the $\epsilon(f)$ best-fit slope with $f$ is consistent with zero. Applying either test gives similar results, and, as the $\mu$ test is more familiar (e.g., Bryan et al. 2003; Jones and Monismith 2008), it is applied here. Because the log spectra are not Gaussian, the least squares standard errors $\varepsilon_\mu$ are approximate, and rigorous statistical tests on $\mu^{(p)}$ and $\mu^{(i)}$ cannot be applied. Instead, quasi-heuristic criteria are used where a data run is rejected if the $\mu$ fit skill $< 0.5$ or if the best fit $\mu$ falls outside of the region

$$\mu - 2\varepsilon_\mu - \Delta < -5/3 < \mu + 2\varepsilon_\mu + \Delta, \tag{7}$$

where $\Delta = 0.06$. Allowing nonzero $\Delta$ gives the test (7) leeway, given the uncertainty of the underlying

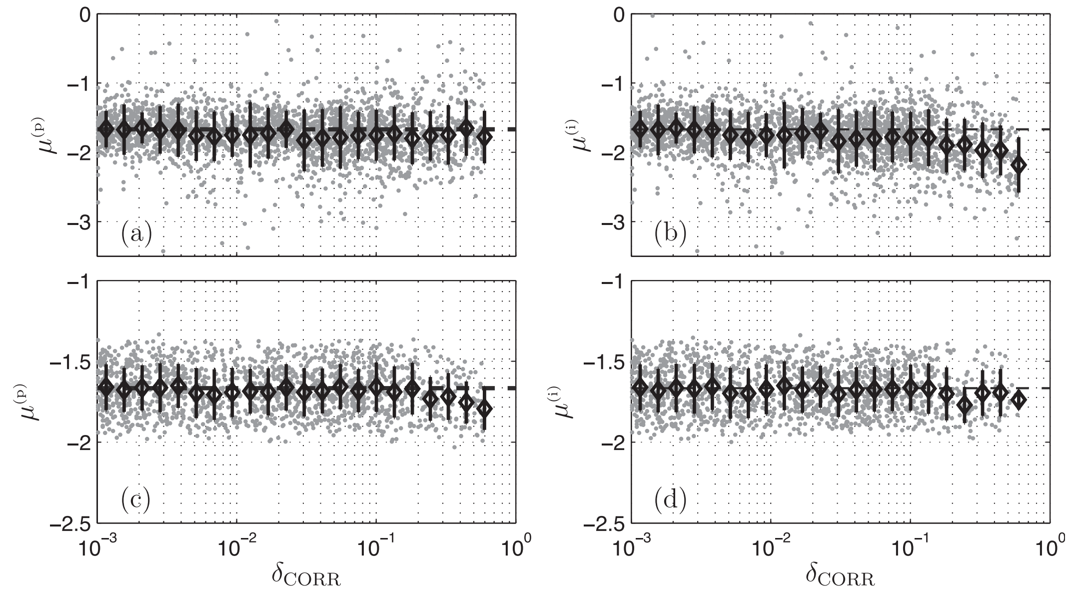


FIG. 9. Vertical velocity spectra $P_{ww}$ power-law exponent (a) $\mu^{(p)}$ and (b) $\mu^{(i)}$ vs $\delta_{CORR}$ for all good-SS data runs ($\delta_{SS} < 0.1$). In (c) $\mu^{(p)}$and (d) $\mu^{(i)}$ vs $\delta_{CORR}$ for cases that additionally pass the $-5/3$ exponent test (7). Individual data points are represented (gray dots) and the binned means (diamonds) and std dev (vertical bars) are shown. The $-5/3$ slope (horizontal dashed black line) is shown. Note the change in vertical scale between (a),(b) and (c),(d). Data runs with $\delta_{CORR} < 10^{-3}$ have similar $\mu^{(p)}$, $\mu^{(i)}$ as at $\delta_{CORR} = 10^{-3}$.

distribution. If the $\mu$ estimates were Gaussian, then $\Delta = 0$ would correspond to 95% confidence limits and, as typically $\varepsilon_\mu \approx 0.12$, $\Delta = 0.06$ corresponds to 99% confidence limits. In general the $\mu^{(p,i)}$ fit skill was high. Only 1.3% and 0.8% of the patched and interpolated data runs, respectively, were rejected owing to low skill. The first case example with $\mu^{(i)} = -1.67 \pm 0.13$ (Fig. 8a) passes the test (7), whereas the second example with $\mu^{(i)} = -2.14 \pm 0.09$ (Fig. 8b) fails. This criterion (7) is applied separately to all $\mu^{(p)}$ and $\mu^{(i)}$ for the good-SS data runs.

The good-$\mu^{(p)}$ data runs [passing the test Eq. (7)] generally fall within the range $-1.9 \le \mu^{(p)} \le -1.4$ (Fig. 9c). The good-$\mu^{(p)}$ binned means are very close to $-5/3$ (diamonds in Fig. 9c), except for $\delta_{CORR} > 0.4$, and the good-$\mu^{(p)}$ binned std dev are reduced to around 0.14 (relative to 0.35 in Fig. 9a). For $\delta_{CORR} > 0.2$, the fit errors $\varepsilon_{\mu^{(p)}}$ are approximately 50% larger than at smaller $\delta_{CORR}$, allowing larger $\mu^{(p)}$ deviation from $-5/3$ to pass the test (7). The $\mu^{(i)}$ that pass (7) have a $\delta_{CORR}$ dependence similar to $\mu^{(p)}$ (cf. Figs. 9d to 9c).

At various $\delta_{CORR}$, between 50% and 80% of the good-SS data runs pass the $\mu^{(p)}$ test (red triangles in Fig. 10). For $\delta_{CORR} < 0.1$, the number $N_\mu$ of good-$\mu$ data runs is basically the same for patching and interpolation, although generally $N_\mu^{(p)}$ is slightly greater than $N_\mu^{(i)}$ (cf. diamonds to triangles in Fig. 10). At $\delta_{CORR} < 10^{-3}$, 80% of patched and interpolated data runs pass the $\mu$ test. Over all $\delta_{CORR}$, 71% and 68% of patched and interpolated good-SS data runs pass the $\mu$ test. However, at larger $\delta_{CORR}$ ($> 0.1$), $N_\mu^{(i)}$ is more clearly reduced relative to $N_\mu^{(p)}$ (cf. diamonds to triangles in Fig. 10), because $\mu^{(i)}$ are biased low (i.e., Fig. 9b), and for binned $\delta_{CORR} > 0.1$, the total $N_\mu^{(p)}$ is 31% greater than the total $N_\mu^{(i)}$.

### 2) RATIO OF HORIZONTAL-TO-VERTICAL VELOCITIES CONSISTENT WITH AN INERTIAL SUBRANGE

Although the power-law exponent $\mu$ test (7) rejects many data runs, some data runs pass with $\delta_{CORR}$ as high as 0.6. To further test the data runs, the second $\overline{\epsilon}$ QC test examines the relationship between horizontal and vertical velocity spectra within an inertial subrange. Previously (Trowbridge and Elgar 2001; Feddersen et al. 2007), the estimated $\overline{\epsilon}$ reliability was determined by checking that the ratio $R \approx 1$, where $R$ is based upon (2) and is defined as

$$R = \frac{(12/21)\langle f^{5/3}P_{uu}(f) + P_{vv}(f) - \text{noise}\rangle}{f^{5/3}P_{ww}(f)}, \qquad (8)$$

where angle brackets represent a frequency average between 1.2 and 2 Hz, and ''noise'' is the $p_{uu} + p_{vv}$ ADV noise level averaged between 3.1 and 4 Hz. For all good-SS data runs, $R^{(p)}$and $R^{(i)}$ are calculated via (8) from the patched and interpolated velocity spectra, respectively. Although $R = 1$ is not strictly required, as the assumptions

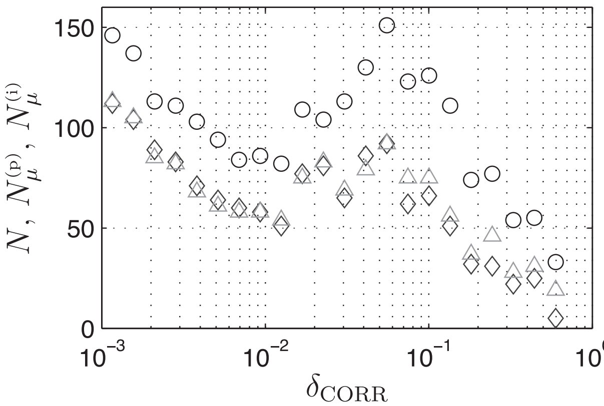


FIG. 10. Binned number of good-SS ($N$, circles), good-$\mu^{(p)}$ ($N_\mu^{(p)}$, triangles), and good-$\mu^{(i)}$ ($N_\mu^{(i)}$, diamonds) data runs vs $\delta_{\rm CORR}$. The variation of good-SS $N$ (circles) with $\delta_{\rm CORR}$ is a result of the instrument locations (cross shore and vertical) and the wave conditions during the experiment.

that go into (2, 8) are violated, the $R$ dependence upon $\delta_{\rm CORR}$ is examined, and $R$ limits are used to reject data runs inconsistent with an inertial subrange.

First, consider the good-SS ($\delta_{\rm SS} < 0.1$) patched and interpolated data runs (Figs. 11a,b). For $\delta_{\rm CORR} < 10^{-2}$, both $R^{(p)}$ and $R^{(i)}$ are generally near unity (binned means between 0.9 and 1.2), but vary at fixed $\delta_{\rm CORR}$ with occasional outliers of $R^{(p,i)} > 3$. For $\delta_{\rm CORR} < 10^{-1}$, $R^{(p)}$ and $R^{(i)}$ binned means increase linearly with $\delta_{\rm CORR}$, the binned std dev also increase, and generally $R^{(p,i)} < 2$. At larger $\delta_{\rm CORR}$ (>0.2), both $R^{(p)}$ and $R^{(i)}$ are typically >2 and both binned means and std dev increase rapidly (Figs. 11a,b). Considering the subset of good-$\mu$ [that pass Eq. (7)] data runs, the overall $R^{(p)}$ and $R^{(i)}$ dependence upon $\delta_{\rm CORR}$ (Figs. 11c,d) is qualitatively similar to that for the good-SS data runs (Figs. 11a,b). The good-$\mu$ data runs remove many of the $R^{(p,i)}$ outliers, resulting in binned means closer to unity and much smaller binned std dev. Thus, the $\mu$ and $R$ tests overlap, as both test for an inertial subrange. At larger $\delta_{\rm CORR}$ (>0.1), the good-$\mu$ $R^{(p)}$ and $R^{(i)}$ binned means increase more slowly than the good-SS $R^{(p,i)}$.

Although (2, 8) are not strictly valid, that $R^{(p)}$ and $R^{(i)}$ are near unity independently indicates that an inertial subrange is often present. Based upon this, data runs that do not satisfy the heuristically chosen criteria $0.5 < R^{(p,i)} < 2$ are rejected (horizontal dashed lines in Fig. 11). For $\delta_{\rm CORR} < 0.1$, very few additional data runs are rejected with this test. At $\delta_{\rm CORR} > 0.2$, many $R^{(p,i)} > 2$, outside of the selected heuristic range. For $\delta_{\rm CORR} > 0.1$, there are $1.5\times$ the number of good-$\mu$–$R$ patched versus interpolated data runs (235 versus 154) and the maximum $\delta_{\rm CORR} = 0.58$ and $\delta_{\rm CORR} = 0.34$ for patching and interpolation, respectively. Thus, at higher $\delta_{\rm CORR}$, patching is more often consistent with an inertial subrange of turbulence and is preferable to interpolation.

## 5. Discussion

### a. Ratio of $\bar\epsilon^{(p)}/\bar\epsilon^{(i)}$

The ratio $\bar\epsilon^{(p)}/\bar\epsilon^{(i)}$ dependence upon $\delta_{\rm CORR}$ is examined to determine their consistency. Ideally, the ratio $\bar\epsilon^{(p)}/\bar\epsilon^{(i)} = 1$. Considering all good-SS data runs, the ratio $\bar\epsilon^{(p)}/\bar\epsilon^{(i)}$ depends upon $\delta_{\rm CORR}$ (Fig. 12a) and generally $\bar\epsilon^{(p)}/\bar\epsilon^{(i)} \ge 1$, as expected. For $\delta_{\rm CORR} < 0.01$, the $\bar\epsilon^{(p)}/\bar\epsilon^{(i)} \approx 1$ (Fig. 12), and the choice of patching or interpolation does not impact $\bar\epsilon$. For $\delta_{\rm CORR} < 0.1$, the binned mean $\bar\epsilon^{(p)}/\bar\epsilon^{(i)}$ slowly increases as does the scatter, but almost always $\bar\epsilon^{(p)}/\bar\epsilon^{(i)} < 1.5$. At larger $\delta_{\rm CORR}$ (>0.2), the binned mean $\bar\epsilon^{(p)}/\bar\epsilon^{(i)}$ increases rapidly, as does the scatter. For the subset of good-$\mu^{(p)}$–$R^{(p)}$ data runs, $\bar\epsilon^{(p)}/\bar\epsilon^{(i)}$ scatter is reduced (Fig. 12b) relative to only good-SS data runs (Fig. 12a). However, the trend of increasing $\bar\epsilon^{(p)}/\bar\epsilon^{(i)}$ at larger $\delta_{\rm CORR}$ (>0.1) is still present. For the good-$\mu^{(p)}$–$R^{(p)}$ data runs, deviations of $\bar\epsilon^{(p)}/\bar\epsilon^{(i)}$ from 1 are due to the effects of interpolation/averaging over longer gaps at higher $\delta_{\rm CORR}$. However, rarely is $\bar\epsilon^{(p)}/\bar\epsilon^{(i)} > 2$. Since $\bar\epsilon$ typically varies over orders of magnitude (here almost three orders of magnitude), the factor of 2 difference between $\bar\epsilon^{(p)}$ and $\bar\epsilon^{(i)}$ further indicates that the good-SS $\mu^{(p)}$–$R^{(p)}$ patched $\bar\epsilon^{(p)}$ are accurate.

### b. Relationship to the p–u coherence test

Previous surf zone ADV QC methodologies (Elgar et al. 2001, 2005) were designed for wave and current studies (frequencies $\lesssim 0.2$ Hz), not for estimating $\bar\epsilon$ (frequencies between 1 and 2 Hz). For example, using a synchronized, collocated pressure measurement, Elgar et al. (2005) require that the swell-band spectral coherence $\overline{C}_{pu}$ between $p$ and $u$ is >0.9, based upon the expectation of <25° surf zone wave directional spread (Kuik et al. 1988). Although many ADV-based surf zone and air–sea boundary $\bar\epsilon$ studies did not have synchronized and collocated pressure measurements (Bryan et al. 2003; Feddersen et al. 2007; Jones and Monismith 2008; Gerbi et al. 2009), such measurements were made during HB06 and the relationship between $\overline{C}_{pu}$ QC criteria and the inertial subrange QC criteria is explored.

Here $\overline{C}_{pu}$ is calculated at all good-SS data runs as the swell band average of the sea surface elevation spectrum-weighted cross-spectral $p$–$u$ coherence $C_{pu}$, that is,

$$\overline{C}_{pu} = \frac{\int_{0.05\rm Hz}^{0.3\rm Hz} C_{pu}(f)P_{\eta\eta}(f)\,df}{\int_{0.05\rm Hz}^{0.3\rm Hz} P_{\eta\eta}(f)\,df},$$

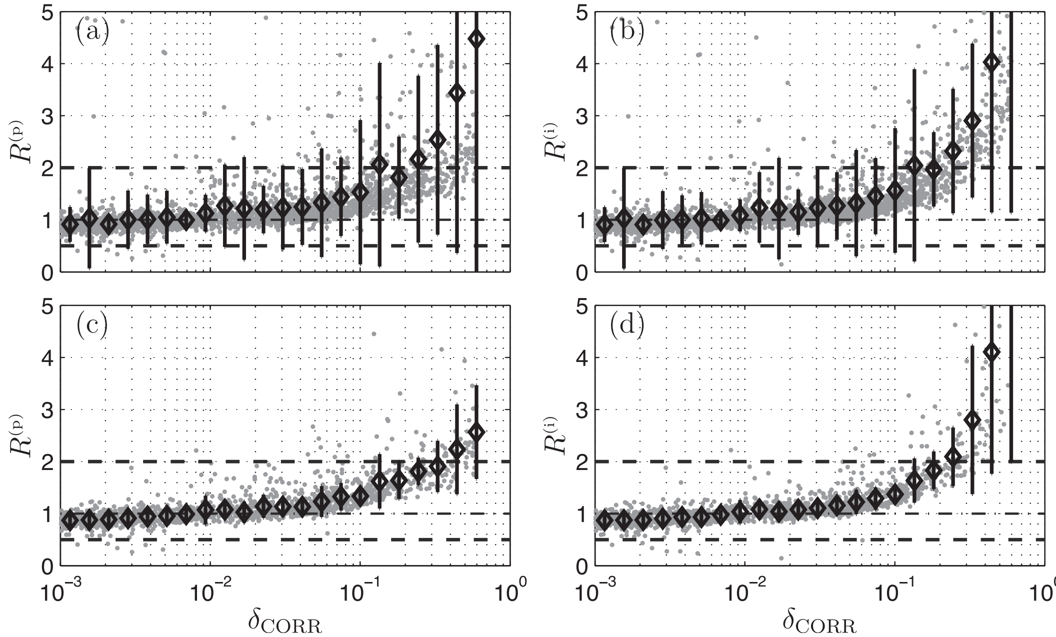


FIG. 11. Plot of (a) $R^{(p)}$ and (b) $R^{(i)}$ vs $\delta_{\mathrm{CORR}}$ at all instruments for the good-SS ($\delta_{\mathrm{SS}} < 0.1$) data runs, and (c) $R^{(p)}$ and (d) $R^{(i)}$ vs $\delta_{\mathrm{CORR}}$ for good-$\mu^{(p)}$ and good-$\mu^{(i)}$ data runs, respectively. Individual data points are represented as gray dots and the binned means (diamonds) and std dev (vertical bars) are shown. $R = 1$ is represented (dashed–dotted horizontal line), as are the $R = 2$ and $R = 0.5$ cutoffs (horizontal dashed lines). Data runs with $\delta_{\mathrm{CORR}} < 10^{-3}$ have $R^{(p)}$, $R^{(i)} \approx 1$ similar as at $\delta_{\mathrm{CORR}} = 10^{-3}$.

where $C_{pu}(f)$ is the spectral $p$–$u$ coherence calculated with $\mu^{(i)}$ and $P_{\eta\eta}$ is the (depth corrected) sea surface elevation spectrum. For the good-SS data runs, $\overline{C}_{pu}$ varies between 0.8 and 1.0 and is largely independent of $\delta_{\mathrm{CORR}}$ (Fig. 13a). The $\overline{C}_{pu} > 0.9$ test (dashed line in Fig. 13a) is failed by 33% of the good-SS data runs. The good-$\mu^{(i)}$–$R^{(p)}$ data runs have a similar $\overline{C}_{pu}$ distribution with $\delta_{\mathrm{CORR}}$ (Fig. 13b) to the good-SS data runs (Fig. 13a). The $\overline{C}_{pu} > 0.9$ test is failed by 31% of these good-$\mu^{(p)}$–$R^{(p)}$ data runs. The bad-$\mu^{(p)}$–$R^{(p)}$ data runs also have a similar $\delta_{\mathrm{CORR}}$ dependence and fail the $\overline{C}_{pu} > 0.9$ test 34% of the time (not shown). Thus, the $\overline{C}_{pu} > 0.9$ test is equally likely to pass or fail for both good and bad $\bar{\epsilon}^{(p)}$ estimates. This applies for other $\overline{C}_{pu}$ thresholds from 0.8 to 1.0, demonstrating that the $\overline{C}_{pu}$ test is not appropriate for quality controlling $\bar{\epsilon}$. Similarly, the $\mu^{(p)}$–$R^{(p)}$ tests based upon the presence of an inertial subrange are not appropriate quality control procedures for estimating wave parameters.

### c. Vertical distribution of good data runs

The vertical distribution of the remaining good data runs is examined to determine where in the water column $\bar{\epsilon}$ can be estimated. For all good-SS data runs, $\mu^{(p)}$ weakly decreases with smaller $z'_{\mathrm{adv}}/a_{\mathrm{sig}}$ (gray dots in Fig. 14a). However, the good-$\mu^{(p)}$ data runs (red dots in Fig. 14a) are independent of $z'_{\mathrm{adv}}/a_{\mathrm{sig}}$, consistent with absence of a good-$\mu^{(p)}$ and $\delta_{\mathrm{CORR}}$ relationship (Figs. 9a,c). For all good-SS data runs, $R^{(p)}$ tends to unity at larger $z'_{\mathrm{adv}}/a_{\mathrm{sig}}$, and $R^{(p)}$ generally increases with increased scatter at smaller $z'_{\mathrm{adv}}/a_{\mathrm{sig}}$ (Fig. 14b), consistent with the relationship between $R^{(p)}$ and $\delta_{\mathrm{CORR}}$ (Fig. 11). The good-$\mu^{(p)}$ values of $R^{(p)}$ also follow this pattern with $z'_{\mathrm{adv}}/a_{\mathrm{sig}}$ (black dots in Fig. 14b). Between $1.2 < z'_{\mathrm{adv}}/a_{\mathrm{sig}} < 2$, about half of the good-$\mu^{(p)}$ data runs are additionally rejected by the $R^{(p)}$ limits (Fig. 14b). At $z'_{\mathrm{adv}}/a_{\mathrm{sig}} > 2$ where most good-$\mu^{(p)}$–$R^{(p)}$ data runs are concentrated, the $R^{(p)}$ cutoff (dashed lines in Fig. 14b) reject only a few additional data runs. Although there are a few good-$\mu^{(p)}$–$R^{(p)}$ data runs as shallow as $z'_{\mathrm{adv}}/a_{\mathrm{sig}} = 1.2$, $\bar{\epsilon}^{(p)}$ can only be consistently estimated at $z'_{\mathrm{adv}}/a_{\mathrm{sig}} > 1.5$. When transformed from sensing volume ($z'_{\mathrm{adv}}$) to transducer ($z'_{\mathrm{tr}}$) coordinates, this results in a limit of $z'_{\mathrm{adv}}/a_{\mathrm{sig}} > 1$, largely corresponding to a stricter SS cutoff of $\delta_{SS} < 10^{-2}$ (Fig. 3), near the Elgar et al. (2005) cutoff of $\delta_{\mathrm{SS}} < 0.008$.

The vertical velocity power-law exponent $\mu$ has been observed to transition from near $-5/3$ to $-1$ within 0.1–0.15 m above the bed (Smyth and Hay 2003) as turbulent eddies become anisotropic. At $z_{\mathrm{adv}} \leq 0.1$ m (sensing volume within 0.1 m of the bed), the binned mean $\mu^{(p)}$ deviates from $-5/3$ and approaches $-1$ (not shown), consistent with Smyth and Hay (2003). In addition, the $R^{(p)}$ values become larger, consistent with anisotropic

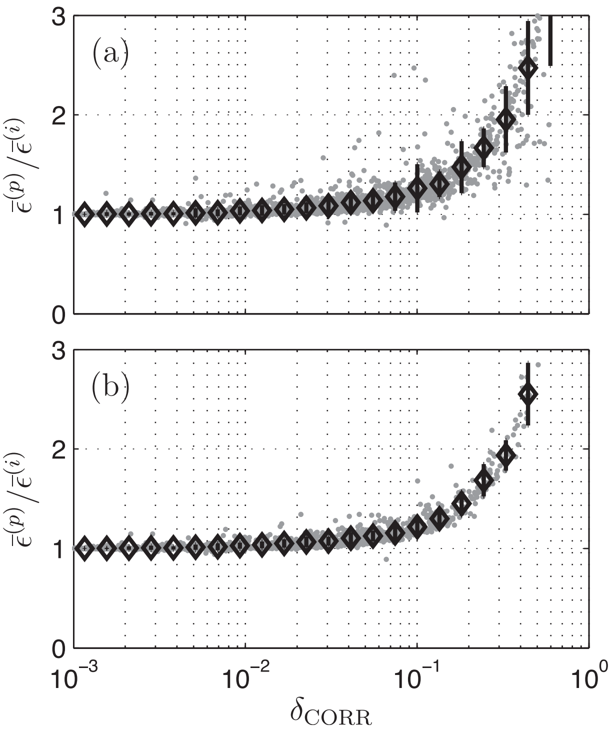


FIG. 12. Plot of $\overline{\epsilon}^{(p)}/\overline{\epsilon}^{(i)}$ vs $\delta_{\mathrm{CORR}}$ at all instruments for (a) good-SS data runs ($\delta_{\mathrm{SS}} < 0.1$) and (b) good-$\mu^{(p)}$–$R^{(p)}$ data runs. The individual data points are represented (gray dots) and the binned means (diamonds) and std dev (vertical bars) are shown. Data runs with $\delta_{\mathrm{CORR}} < 10^{-3}$ have $\overline{\epsilon}^{(p)}/\overline{\epsilon}^{(i)} \approx 1$ similar as at $\delta_{\mathrm{CORR}} = 10^{-3}$.

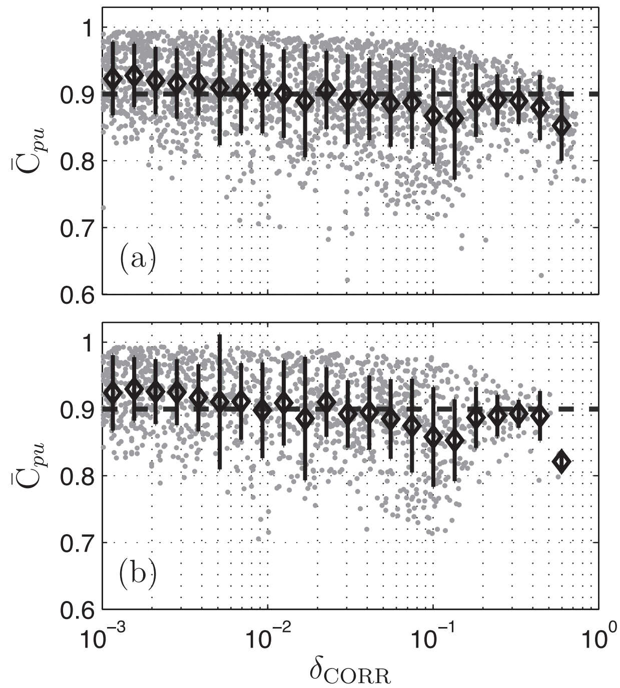


FIG. 13. Plot of $\overline{C}_{pu}$ vs $\delta_{\mathrm{CORR}}$ at all instruments for (a) good-SS data runs ($\delta_{\mathrm{SS}} < 0.1$) and (b) good-$\mu^{(p)}$–$R^{(p)}$ data runs. The individual data points are represented (gray dots) and the binned means (diamonds) and std dev (vertical bars) are shown. The dashed horizontal line at $\overline{C}_{pu} = 0.9$ indicates the Elgar et al. (2005) cutoff. Data runs with $\delta_{\mathrm{CORR}} < 10^{-3}$ have a similar $\overline{C}_{pu}$ pattern similar as at $\delta_{\mathrm{CORR}} = 10^{-3}$.

eddies. Therefore, few (22 out of 146; i.e., 15%) data runs passed both QC tests at $z_{\mathrm{adv}} < 0.1$. At $z_{\mathrm{adv}} > 0.1$ m, no change in $\mu^{(p)}$ or $R^{(p)}$ was observed. Thus $z_{\mathrm{adv}} = 0.1$ m is a lower near-bed limit where $\overline{\epsilon}^{(p)}$ can be estimated.

The $z'_{\mathrm{adv}}/a_{\mathrm{sig}} > 1.5$ limit is useful in designing an open ocean air–sea boundary layer studies (e.g., Gerbi et al. 2009). The surf zone is a region of overlapping surface and bottom boundary layers, and from this alone the water column range in which $\overline{\epsilon}^{(p)}$ can be estimated is not clear. Within a saturated (self-similar) surf zone, where $H_{\mathrm{sig}} = \gamma h$ in which $\gamma \approx 0.5$ (Raubenheimber et al. 1996), the $z'_{\mathrm{adv}}/a_{\mathrm{sig}} \approx 1.5$ limit results in a water column limit $z_{\mathrm{adv}}/h \lesssim 0.6$. Thus, turbulent dissipation rate $\epsilon$ can be consistently estimated in the lower 60% of the water column and more than 0.1 m above the bed within a saturated surf zone.

## 6. Summary

A quality control methodology for estimating surf-zone turbulent dissipation rate $\epsilon$ from ADV observations is presented and applied to the HB06 experiment data. First, ADV velocity measurements are quality controlled using the ADV backscattered signal strength (SS) and correlation signal (CORR) to identify bad velocity data points. The fraction of bad SS data points $\delta_{\mathrm{SS}}$ increases inversely with the (wave amplitude) normalized ADV transducer distance to the mean sea surface, consistent with exposure out of water as the dominant reason for bad SS. Based on statistics of the data-gap length, a liberal cutoff criteria of $\delta_{\mathrm{SS}} > 0.1$ is preliminarily chosen to reject data runs. The fraction of bad CORR data points $\delta_{\mathrm{CORR}}$ can be significant even when $\delta_{\mathrm{SS}}$ is small. The $\delta_{\mathrm{CORR}}$ is a function of both the (wave amplitude) normalized ADV sensing volume distance below the mean sea surface and also the wave energy flux gradient, consistent with turbulence- and bubble-induced Doppler noise.

Turbulent dissipation rate $\overline{\epsilon}$ is estimated from vertical velocity spectra derived from both patched and interpolated time series. Two QC tests, based upon the properties of the expected turbulent inertial subrange are applied to reject bad $\overline{\epsilon}$ data runs. The first test uses the vertical velocity spectrum's power-law exponent $\mu$, expected to be $-5/3$ in an inertial subrange. The second test checks that a ratio $R$ of horizontal and vertical velocity spectra band is consistent with an inertial subrange. For $\delta_{\mathrm{CORR}} < 0.1$, between 60% and 80% of

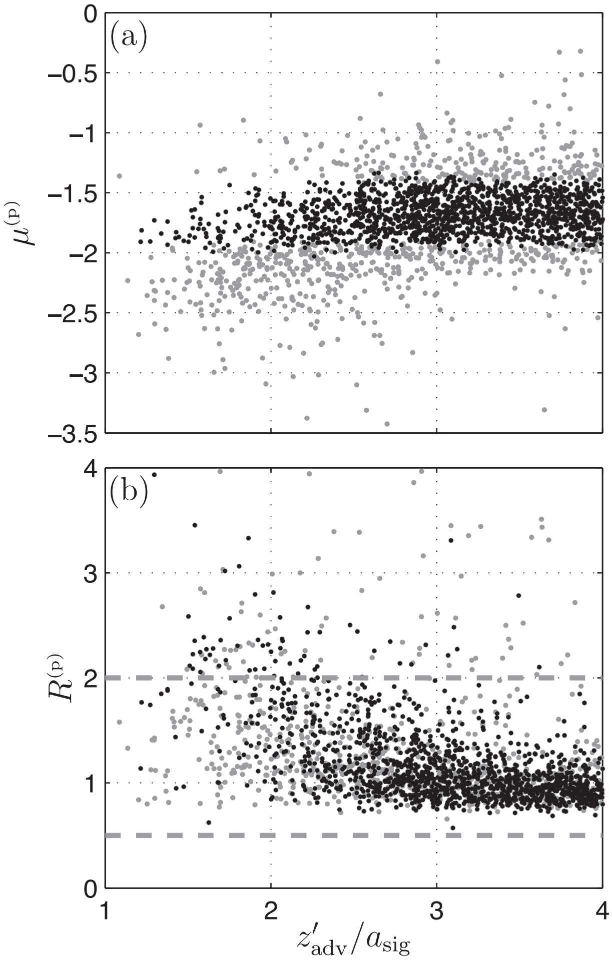


FIG. 14. Plot of (a) $\mu^{(p)}$and (b) $R^{(p)}$vs $z'_{\mathrm{adv}}/a_{\mathrm{sig}}$. The good-SS data runs (gray) and the good-$\mu^{(p)}$ data runs (black) are shown. In (b), the dashed horizontal lines indicate the $R^{(p)}$ cutoffs.

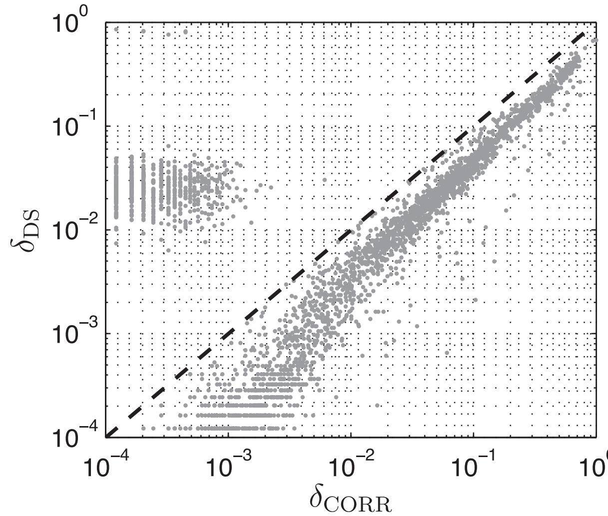


FIG. A1. Plot of $\delta_{\mathrm{DS}}$ vs $\delta_{\mathrm{CORR}}$ for all good-SS ($\delta_{\mathrm{SS}} < 0.1$) data runs at all instruments. The dashed line is the 1:1 relationship.

patched and interpolated data runs pass these tests. At larger $\delta_{\mathrm{CORR}}$ (>0.1), 50% more patched than interpolated data runs pass the tests, and patched data runs are used. Of the remaining data runs, the ratio of patched-to-interpolated dissipation $\bar{\epsilon}^{(p)}/\bar{\epsilon}^{(i)}$ is generally near unity. Prior surf zone ADV QC methodologies designed for wave studies (frequencies $\lesssim$0.2 Hz) have no predictive skill in rejecting bad $\bar{\epsilon}$ data runs. The resulting good $\bar{\epsilon}^{(p)}$ data runs distributed at normalized vertical locations $z'_{\mathrm{adv}}/a_{\mathrm{sig}} > 1.5$. This suggests that the turbulent dissipation rate can be consistently estimated over the lower 60% of the water column and >0.1 m above the bed within a saturated (self-similar) surf zone.

*Acknowledgments.* The HB06 experiment and this research was supported by CA Coastal Conservancy, NOAA, ONR, NSF, and CA Sea Grant. R. T. Guza was co-PI on the HB06 experiment. Staff and students from the Integrative Oceanography Division (B. Woodward, B. Boyd, K. Smith, D. Darnell, I. Nagy, D. Clark, M. Omand, M. Yates, M. McKenna, M. Rippy, S. Henderson, and M. Spydell) were instrumental in acquiring the field observations for this research. In addition, R. T. Guza, Gerben Ruessink, G. Gerbi, and Peter Sutherland provided feedback on this work.

## APPENDIX

### Comparison of the Correlation and Despike QC Methods

Other QC methodologies have been developed that only use ADV velocities to determine the bad data points, often called ''spikes.'' Common strategies include rejecting data more than a certain number of standard deviations from the mean, or removing data points where the acceleration (velocity first difference) exceed some threshold. Phase space quality control methods (Goring and Nikora 2002; Wahl 2003) combine these strategies by calculating a 3D ellipsoid that fits the observed velocity component ($u$) and their first ($\Delta u$) and second ($\Delta^2 u$) differences (where $\Delta$ is the difference operator) on the three axes. Data points outside the fit ellipsoid are considered bad (or spikes) and are rejected. This process is iterated until no more data points lie outside the ellipse.

The application of phase space (or despiking) methods to ADV data is most common in hydraulic engineering (e.g., Lacey and Roy 2008) and estuarine studies (e.g., Trevethan and Chanson 2009). In bubbly laboratory surfzone turbulence studies (e.g., Mori et al. 2007a), phase space quality control methods (Goring and Nikora 2002) work well in removing erroneous ADV data spikes (Mori et al. 2007b). Despiking methods are also combined with the ADV SS and CORR methods (e.g., Chanson et al. 2008).

Here the fraction of bad data points from the CORR ($\delta_{\mathrm{CORR}}$) and despiking ($\delta_{\mathrm{DS}}$) QC methods are compared. The despiking QC applies the algorithm of Goring and Nikora (2002) as applied by Mori et al. (2007b) subsequent to removal of data points with SS $<$ 100 counts and CORR $<$ 0.3 (minimum CORR for mean flow estimation; SonTek 2004). The two QC methods generally give similar $\delta_{\mathrm{DS}}$ and $\delta_{\mathrm{CORR}}$ (Fig. A1) with $\delta_{\mathrm{DS}}$ usually slightly less than $\delta_{\mathrm{CORR}}$ (most data fall just below the dashed 1:1 line). For these cases, the bad CORR data points are a superset of the bad despiked data. There is also a data cloud near $\delta_{\mathrm{DS}} \approx 10^{-2}$ and $\delta_{\mathrm{CORR}} \approx 10^{-4}$–$10^{-3}$ far from the 1:1 relationship (Fig. A1) that includes about 30% of the observations. The cause of the elevated $\delta_{\mathrm{DS}}$ at these low $\delta_{\mathrm{CORR}}$ is unclear but may be related to fitting a Gaussian envelope to a nonlinear wave field.

## REFERENCES


Apotsos, A., B. Raubenheimer, S. Elgar, and R. T. Guza, 2008: Wave-driven setup and alongshore flows observed onshore of a submarine canyon. *J. Geophys. Res.,* **113,** C07025, doi:10.1029/2007JC004514.

Batchelor, G. K., 1953: *The Theory of Homogeneous Turbulence*. Cambridge University Press, 197 pp.

Beach, R. A., and R. W. Sternberg, 1996: Suspended-sediment transport in the surf zone: Response to breaking waves. *Cont. Shelf Res.,* **16,** 1989–2003.

Bryan, K. R., K. P. Black, and R. M. Gorman, 2003: Spectral estimates of dissipation rate within and near the surf zone. *J. Phys. Oceanogr.,* **33,** 979–993.

Cabrera, R., K. Deines, B. Brumley, and E. Terray, 1987: Development of a practical coherent acoustic Doppler current profiler. *Proc. Oceans* '87, Halifax, NS, Canada, IEEE Ocean Engineering Society, 93–97.

Chanson, H., M. Trevethan, and S. Aoki, 2008: Acoustic Doppler velocimetry (ADV) in small estuary: Field experience and signal post-processing. *Flow Meas. Instrum.,* **19,** 307–313, doi:10.1016/j.flowmeasinst.2008.03.003.

Clark, D. B., F. Feddersen, and R. T. Guza, 2010: Cross-shore surfzone tracer dispersion in an alongshore current. *J. Geophys. Res.,* **115,** C10035, doi:10.1029/2009JC005683.

Deane, G. B., and M. D. Stokes, 2002: Scale dependence of bubble creation mechanisms in breaking waves. *Nature,* **418,** 839–844.

Elgar, S., B. Raubenheimer, and R. T. Guza, 2001: Current meter performance in the surf zone. *J. Atmos. Oceanic Technol.,* **18,** 1735–1746.

——, ——, and ——, 2005: Quality control of acoustic Doppler velocimeter data in the surfzone. *Meas. Sci. Technol.,* **16,** 1889–1893.

Feddersen, F., and J. H. Trowbridge, 2005: The effect of wave breaking on surf-zone turbulence and alongshore currents: A modeling study. *J. Phys. Oceanogr.,* **35,** 2187–2204.

——, ——, and A. J. Williams, 2007: Vertical structure of dissipation in the nearshore. *J. Phys. Oceanogr.,* **37,** 1764–1777.

Garret, C., M. Li, and D. Farmer, 2000: The connection between bubble size spectra and energy dissipation rates in the upper ocean. *J. Phys. Oceanogr.,* **30,** 2163–2171.

George, R., R. E. Flick, and R. T. Guza, 1994: Observations of turbulence in the surf zone. *J. Geophys. Res.,* **99,** 801–810.

Gerbi, G. P., J. H. Trowbridge, E. A. Terray, A. J. Plueddemann, and T. Kukulka, 2009: Observations of turbulence in the ocean surface boundary layer: Energetics and transport. *J. Phys. Oceanogr.,* **39,** 1077–1096.

Goring, D. G., and V. I. Nikora, 2002: Despiking acoustic Doppler velocimeter data. *J. Hydraul. Eng.,* **128,** 117–126.

Guza, R. T., and E. B. Thornton, 1980: Local and shoaled comparisons of sea surface elevations, pressures, and velocities. *J. Geophys. Res.,* **85,** 1524–1530.

——, and ——, 1985: Observations of surf beat. *J. Geophys. Res.,* **90,** 3161–3172.

Jones, N. L., and S. G. Monismith, 2008: The influence of whitecapping waves on the vertical structure of turbulence in a shallow estuarine embayment. *J. Phys. Oceanogr.,* **38,** 1563–1580.

Kim, S., C. Friedrichs, J. Maa, and L. Wright, 2000: Estimating bottom stress in tidal boundary layer from Acoustic Doppler Velocimeter data. *J. Hydraul. Eng.,* **126,** 399–406.

Kuik, A. J., G. P. V. Vledder, and L. H. Holthuijsen, 1988: A method for the routine analysis of pitch-and-roll buoy wave data. *J. Phys. Oceanogr.,* **18,** 1020–1034.

Lacey, R. W. J., and A. G. Roy, 2008: Fine-scale characterization of the turbulent shear layer of an instream pebble cluster. *J. Hydraul. Eng.,* **134,** 925–936, doi:10.1061/(ASCE)0733-9429(2008)134:7(925).

Lhermitte, R., and U. Lemmin, 1994: Open-channel flow and turbulence measurement by high-resolution Doppler sonar. *J. Atmos. Oceanic Technol.,* **11,** 1295–1308.

Lohrmann, A., R. Cabrera, and N. Kraus, 1994: Acoustic-Doppler velocimeter (ADV) for laboratory use. *Proc. Conf. on Fundamentals and Advancements in Hydraulic Measurements and Experimentation,* Buffalo, NY, Hydraulics Division ASCE, 351–365.

Lumley, J. L., and E. A. Terray, 1983: Kinematics of turbulence convected by a random wave field. *J. Phys. Oceanogr.,* **13,** 2000–2007.

Martin, V., T. S. R. Fisher, R. G. Millar, and M. C. Quick, 2002: ADV data analysis for turbulent flows: Low correlation problem. *Proc. Hydraulic Measurements and Experimental Methods 2002,* Estes Park, CO, Environmental and Water Resources Institute of ASCE and International Association of Hydraulic Engineering and Research, doi:10.1061/40655(2002)101.

Mori, N., T. Suzuki, and S. Kakuno, 2007a: Experimental study of air bubbles and turbulence characteristics in the surf zone. *J. Geophys. Res.,* **112,** C05014, doi:10.1029/2006JC003647.

——, ——, and ——, 2007b: Noise of acoustic Doppler velocimeter data in bubbly flows. *J. Eng. Mech.,* **133,** 122–125, doi:10.1061/(ASCE)0733-9399(2007)133:1(122).

Raubenheimber, B., S. Elgar, and R. T. Guza, 1996: Wave transformation across the inner surf zone. *J. Geophys. Res.,* **101,** 25 589–25 597.

——, ——, and ——, 1998: Estimating wave heights from pressure measured in a sand bed. *J. Waterw. Port Coastal Ocean Eng.,* **124,** 151–154.

——, ——, and ——, 2004: Observations of swash zone velocities: A note on friction coefficients. *J. Geophys. Res.,* **109,** C01027, doi:10.1029/2003JC001877.

Scott, C. P., D. T. Cox, T. B. Maddux, and J. W. Long, 2005: Large-scale laboratory observations of turbulence on a fixed barred beach. *Meas. Sci. Technol.,* **16,** 1903–1912.

Sheremet, A., R. T. Guza, and T. H. C. Herbers, 2005: A new estimator for directional properties of nearshore waves. *J. Geophys. Res.,* **110,** C01001, doi:10.1029/2003JC002236.

Smyth, C., and A. Hay, 2003: Near-bed turbulence and bottom friction during SandyDuck97. *J. Geophys. Res.,* **108,** 3197, doi:10.1029/2001JC000952.

SonTek, 2004: SonTek ADVField Acoustic Doppler Velocimeter: Technical documentation. SonTek/YSI, San Diego, CA, 186 pp.

Spydell, M. S., F. Feddersen, and R. T. Guza, 2009: Observations of drifter dispersion in the surfzone: The effect of sheared alongshore currents. *J. Geophys. Res.,* **114,** C07028, doi:10.1029/2009JC005328.

Terray, E. A., M. A. Donelan, Y. C. Agrawal, W. M. Drennan, K. K. Kahma, A. J. Williams, P. A. Hwang, and S. A. Kitaigorodskii, 1996: Estimates of kinetic energy dissipation under breaking waves. *J. Phys. Oceanogr.,* **26,** 792–807.

Thomson, J., S. Elgar, T. H. C. Herbers, B. Raubenheimer, and R. T. Guza, 2007: Refraction and reflection of infragravity waves near submarine canyons. *J. Geophys. Res.,* **112,** C10009, doi:10.1029/2007JC004227.

Trevethan, M., and H. Chanson, 2009: Turbulent mixing in a small estuary: Detailed measurements. *Estuarine Coastal Shelf Sci.,* **81,** 191–200, doi:10.1016/j.ecss.2008.10.020.

Trowbridge, J., and S. Elgar, 2001: Turbulence measurements in the surf zone. *J. Phys. Oceanogr.,* **31,** 2403–2417.

Voulgaris, G., and J. H. Trowbridge, 2001: Evaluation of the acoustic Doppler velocimeter (ADV) for turbulence measurements. *J. Atmos. Oceanic Technol.,* **15,** 272–289.

Wahl, T. L., 2003: Discussion of ''despiking acoustic Doppler velocimeter data'' by D. G. Goring and V. I. Nikora. *J. Hydraul. Eng.,* **129,** 484–487.

Zedel, L., A. E. Hay, R. Cabrera, and A. Lohrmann, 1996: Performance of a single-beam pulse-to-pulse coherent Doppler profiler. *IEEE J. Oceanic Eng.,* **21,** 290–297, doi:10.1109/48.508159.